

Is $\text{MgII}\lambda 2800$ a Reliable Virial Broadening Estimator for Quasars?

Paola Marziani^{1,2}, Jack W. Sulentic², Ilse Plauchu-Frayn^{2,*} and Ascensión del Olmo²

¹ INAF, Osservatorio Astronomico di Padova, Padova, Italy
e-mail: paola.marziani@oapd.inaf.it

² Instituto de Astrofísica de Andalucía, CSIC, Granada, España

ABSTRACT

Context. Broad $\text{MgII}\lambda 2800$ and $\text{H}\beta$ lines have emerged as the most reliable virial estimators of black hole mass in quasars. Which is more reliable? Part of the challenge centers on comparing $\text{MgII}\lambda 2800$ and $\text{H}\beta$ line profiles in order to improve the ± 1 dex M_{BH} uncertainties inherent in single-epoch FWHM measures from noisy spectra.

Aims. Comparison of $\text{MgII}\lambda 2800$ and $\text{H}\beta$ profile measures in the same sources and especially FWHM measures that provide the virial broadening estimator.

Methods. Identification of 680 bright Sloan Digital Sky Survey DataRelease 7 quasars with spectra showing both $\text{MgII}\lambda 2800$ and $\text{H}\beta$ lines, at redshift $0.4 \leq z \leq 0.75$. The s/n of these spectra are high enough to allow binning in the “four-dimensional (4D) eigenvector 1” optical plane and construction of high s/n composite spectra.

Results. We confirm that $\text{MgII}\lambda 2800$ shows a profile that is $\approx 20\%$ narrower as suggested in some previous studies. FWHM measures for Population B sources (i.e., with FWHM of $\text{H}\beta$ larger than 4000 km s^{-1}) are uncertain because they show complex profiles with at least two broad-line components involving a nearly unshifted broad and redshifted very-broad component. Only the broad component is likely to be a valid virial estimator. If $\text{H}\beta$ and $\text{MgII}\lambda 2800$ are not corrected for the very broad component then black hole mass M_{BH} values for Population B sources will be systematically overestimated by up to $\Delta \log M_{\text{BH}} \approx 0.3 - 0.4$ dex. We suggest a simple correction that can be applied to the majority of sources. $\text{MgII}\lambda 2800$ is the safer virial estimator for Population B sources because the centroid shifts with respect to rest frame are lower than for $\text{H}\beta$. In the broad and very broad component profile interpretation this is a consequence of the lower very broad to broad component intensity ratio for $\text{MgII}\lambda 2800$. Eigenvector-based studies show that effective discrimination of black hole mass and Eddington ratio at fixed redshift is not achieved via luminosity binning but rather by binning in a “4D eigenvector 1” context that reflects different broad line region geometry/kinematics likely driven by Eddington ratio.

Key words. quasars: general – quasars: emission lines – line: profiles – black hole physics

1. Introduction

Estimations of black hole mass (M_{BH}) and Eddington ratio (L/L_{Edd}) for large and diverse samples of quasars (Marziani & Sulentic 2012; Shen 2013, and references therein) are

*Now at Instituto de Astronomía, UNAM, Ensenada Campus, Baja California, México

needed for both astrophysical and cosmological studies. Until recently the majority of virial black hole M_{BH} estimates have not taken profile diversity into account. Rather, broad-line FWHM measures have been assumed to be valid virial estimators in all quasars. The situation becomes even more complicated when we compare FWHM estimates derived from different lines that often show quite different profile shapes (e.g., Barthel et al. 1990; Baskin & Laor 2005; Brotherton et al. 1994; Ho et al. 2012; Wills et al. 1993; Zamfir et al. 2010). The goal of the present paper is to systematize differences between $\text{H}\beta$ and $\text{MgII}\lambda 2800$ in the process of comparing the relative merits of FWHM $\text{H}\beta$ and $\text{MgII}\lambda 2800$ as virial broadening estimators. This is done within the context of a 4D Eigenvector 1 parameter formalism.

1.1. The 4D eigenvector 1 parameter space

Interpretation of quasar spectra in the context of a 4D parameter space stemming from eigenvector studies reveals a large diversity of line profile properties (Marziani et al. 2010, 2003b; Sulentic et al. 2007, 2000a) likely driven by L/L_{Edd} , with M_{BH} and source orientation also playing important roles (Boroson & Green 1992; Marziani et al. 2001; Yip et al. 2004). The 4DE1 (4D Eigenvector 1) formalism owes its inception to a principal component analysis study of systematic trends in quasar spectra (Boroson & Green 1992) from the Palomar-Green (PG) survey. The first eigenvector (E1) included a correlation between $[\text{OIII}]\lambda\lambda 4959, 5007$ and optical FeII strength and an anti-correlation between the latter parameter and FWHM $\text{H}\beta$. Variants of E1 were later found in several studies (e.g. Boroson 2002; Grupe 2004; Kovačević et al. 2010; Kruczek et al. 2011; Kuraszkiewicz et al. 2002; Marziani et al. 1996; Sulentic et al. 2002, 2000b; Tang et al. 2012; Wang et al. 2006; Yip et al. 2004). E1 was eventually expanded into 4DE1 parameter space (Sulentic et al. 2007, 2000a) with the addition $\text{CIV}\lambda 1549$ profile shift and soft X-ray photon index as important parameters that show some of the strongest intercorrelations. The higher dimensionality involves parameters that are observationally independent and that correspond to different physical processes (see the reviews by Sulentic et al. 2000a and Marziani & Sulentic 2012 for more detailed discussions). Quasars occupy a well defined sequence in the “optical plane” of 4DE1 defined by the FWHM of the $\text{H}\beta$ broad component and by the intensity ratio between $\text{FeII}\lambda 4570$ and $\text{H}\beta$ (Boroson & Green 1992; Sulentic et al. 2002). The 4DE1 optical plane therefore offers a tool that allows for the definition and identification of quasar populations or spectral types.

1.2. Two main quasar populations

Exploration of the 4DE1 parameter space gave rise to the concept of two quasar populations that, if not truly distinct, are an effective way to distinguish important spectroscopic differences between quasars. Pop. A sources show a wide range of broad-line widths (FWHM $\text{H}\beta \sim 600 - 4000 \text{ km s}^{-1}$) with a majority of sources (in low redshift samples) between FWHM $\text{H}\beta \sim 1000 - 4000 \text{ km s}^{-1}$. Few sources with $R_{\text{FeII}} > 0.5$ show FWHM $\text{H}\beta > 4000 \text{ km s}^{-1}$ which was partial motivation for the Pop. A-B formalism. Pop. A involves a largely radio-quiet quasar population as few radio-loud quasars (especially with double-lobe Fanaroff-Riley II (FRII) radio morphology) show FWHM $\text{H}\beta < 4000 \text{ km s}^{-1}$ (Zamfir et al. 2008). AGN with FWHM $\text{H}\beta \leq 2000 \text{ km s}^{-1}$ are often referred to as narrow line Seyfert 1 (NLSy1) sources but there is continuity in source properties over the full Pop. A range of FWHM $\text{H}\beta$. The “Population A” definition changes in higher redshift samples because the minimum observed broad-line FWHM of $\text{H}\beta$ slowly increases with source luminosity (see Figure 11 in Marziani et al. 2009, and Dultzin et al. 2011). Pop. A $\text{H}\beta$ profiles are best fit with a single symmetric Lorentz function while Pop. B are not. Following previous results for $\text{H}\beta$ we fit all Pop. A $\text{MgII}\lambda 2800$ profiles with Lorentz

functions (Sulentic et al. 2002; Véron-Cetty et al. 2001). Pop. B quasars show an even wider range of FWHM H β than Pop. A sources. The full observed range is FWHM H β = 4000 – 40000 km s $^{-1}$ (Wang et al. 2009), but values FWHM H β > 16000 km s $^{-1}$ are extremely rare with almost all sources in a low redshift sample between 4000 km s $^{-1}$ and 12000 km s $^{-1}$. Most Pop. B sources show $R_{\text{FeII}} < 0.5$. Pop B is a mixed radio-quiet and radio-loud population with the majority of radio-loud sources within population B. Pop. B sources are different from Pop. A because – most fundamentally – they show composite H β profiles. The majority of Pop. B H β profiles can be modelled with an (almost) unshifted broad (BC) and redshifted very broad component (VBC). It is usually assumed that the unshifted BC is the same as the single component observed in Pop. A sources while the VBC is something non-virial and apparently unique to Pop. B sources (both radio-quiet and radio-loud). Further discussion on Pop. A and B is provided by Sulentic et al. (2011).

1.3. Black hole mass estimates

The equation used to estimate M_{BH} can be written, under the assumption that line broadening in quasars is due to virialized motions in the emitting gas, as:

$$M_{\text{BH}} = \mathcal{F} \frac{r_{\text{BLR}} (\Delta v)^2}{G} \quad (1)$$

where \mathcal{F} is factor ≈ 1 that depends on geometry of the emitting gas (e.g., Graham et al. 2011; Onken et al. 2004), r_{BLR} is an emissivity-weighted radial distance of the broad line emitting region (BLR), and Δv is the virial broadening term, customarily measured from the width of a suitable emission line. The most accurate M_{BH} estimates come from reverberation mapping measures of r_{BLR} (e.g. Denney et al. 2009; Horne et al. 2004) coupled with H β rms profile widths (FWHM or velocity dispersion σ ; Peterson et al. 2004). We now have ≈ 60 reverberation derived radii (Bentz et al. 2013, 2009, 2010). The cost in telescope time for such accurate r_{BLR} and rms line width estimates is very high even for the brightest sources. It is clear that we must rely on secondary methods in order to obtain a large numbers of additional M_{BH} estimates, as needed for the analysis of an ever increasing population of catalogued quasars (Ross et al. 2012; Schneider et al. 2010). These methods involve single-epoch FWHM measures and r_{BLR} estimates derived from the apparent correlation between reverberation derived radii and source luminosity measures (the so-called “Kaspi relation;” Kaspi et al. 2005). We suggest that line measures for large source samples can be better utilized if 4D parameter space coordinates for each source are taken into account. This is especially true if 4DE1 coordinates are driven by source Eddington ratio.

Important issues connected with the use of Eq. 1 involve: 1) the validity of extrapolating the Kaspi relation beyond the range of redshift and source luminosity represented in the reverberation sample and 2) estimation of the virial broadening Δv . There are two sides to virial broadening estimation: a) the choice of a suitable emission line (assumed primarily broadened by virial motions) and b) selection of a suitable parameter (FWHM, σ) to define the virial broadening Δv . Single-epoch FWHM H β measures have provided M_{BH} estimates for large samples at low and high redshifts. Measures of the second moment σ are less useful in the case of a broad lines with more than one component. Beyond redshift $z \gtrsim 0.7$ we lose the most trusted source of single-epoch FWHM measures (i.e. H β). We can either follow H β into the infrared and/or adopt FWHM measures of other broad lines as virial estimators. We have adopted the former approach taking advantage of Very Large Telescope (VLT) ISAAC (Moorwood et al. 1998) spectroscopy to follow H β through the IR windows and obtain accurate as possible M_{BH} estimates for ≈ 50 luminous quasars in the range $z \approx 1.0 - 3.0$ (Marziani et al. 2009; Sulentic et al. 2006, 2004). We are currently

processing a sample of ≈ 25 sources where $H\beta$ is redshifted into the K band window ($z \approx 3.0 - 3.7$) beyond which $H\beta$ is lost (Sulentic et al. 2013 in preparation).

1.4. Use of $MgII\lambda 2800$

The strongest available surrogate broad lines that are redshifted into the optical over a wide z range are $CIV\lambda 1549$ and $MgII\lambda 2800$. The region of $CIII]\lambda 1909$ is a blend of permitted and semi-forbidden lines whose apparent intricacy has deterred previous workers although there is potential for progress if moderate resolution high s/n spectra are available (Marziani et al. 2011, 2010; Negrete et al. 2012; Negrete 2011). $CIV\lambda 1549$ is not recommended as a virial estimator because FWHM $CIV\lambda 1549$ does not even show a correlation with FWHM $H\beta$ (Marziani et al. 1996; Netzer et al. 2007; Richards et al. 2011; Shen et al. 2008; Sulentic et al. 2007). $CIV\lambda 1549$ also shows a blueshift and profile asymmetry in many sources (Brotherton 1996; Gaskell 1982; Richards et al. 2011; Sulentic et al. 2007) challenging the validity of the virial assumption. Some consistency can be achieved if several cautions and corrections are applied to the $CIV\lambda 1549$ measures (Assef et al. 2011; Denney 2012; Greene et al. 2010, and especially in the 4DE1 context as done by Sulentic et al. 2007) but this is not the road to M_{BH} estimates with uncertainties less than 1dex. In the 4DE1 context (Sulentic et al. 2000b) both $H\beta$ and $CIV\lambda 1549$ show strikingly different profile properties for Pop. A and B sources. Such differences cannot be easily quantified with low resolution and/or low s/n spectra.

The rest wavelength of $MgII\lambda 2800$ makes it a potentially valuable ground-based virial estimator from $z \approx 0.4$ up to $z \approx 2.1$. Rapid improvements in IR spectroscopy also makes $MgII\lambda 2800$ accessible at higher redshifts. It has been measured in K band for the quasar with highest known redshift $z \approx 7.085$ redshift (Mortlock et al. 2011). Is $MgII\lambda 2800$ a safe $H\beta$ surrogate? $Mg^+ \lambda\lambda 2796, 2803$ is a low ionization line (LIL) doublet long thought to be produced in a dense optically-thick region where at least part of the Balmer lines arise (Grandi & Phillips 1979; Netzer 1980). A possible complication is that $MgII\lambda 2800$ is a resonance line and therefore often affected by broad (Ganguly & Brotherton 2008) and narrow absorption (Wild et al. 2008). Several authors have attempted to define a relation between $MgII\lambda 2800$ and $H\beta$ to provide consistent M_{BH} estimates from the two lines (McLure & Jarvis 2002; Shen & Liu 2012; Trakhtenbrot & Netzer 2012; Vestergaard & Peterson 2006; Wang et al. 2009). $MgII\lambda 2800$ is assumed to be a virial estimator as reliable as $H\beta$ because their line widths are correlated. Latest studies however show considerable scatter (and deviation from parity) in the FWHM $H\beta$ vs. FWHM $MgII\lambda 2800$ correlation. There is strong evidence that FWHM $MgII\lambda 2800$ is about 20% smaller than FWHM $H\beta$ (Wang et al. 2009) in many sources.

We report here on a more detailed comparison of $H\beta$ and $MgII\lambda 2800$ as virial estimators. This work goes beyond several recent works considering line shape properties (shifts and asymmetries, presence of a very broad component) that could weaken or invalidate the virial assumption. Such a more detailed study requires separate consideration of sources with FWHM $H\beta$ less than or greater than 4000 km s^{-1} (Population A and B respectively; cf. Pop. 1 and 2 of Collin et al. 2006). Results for Pop. A sources were presented in a companion paper (Marziani et al. 2013, hereafter Paper I). The majority ($\approx 80\%$) of Pop. A sources show an unshifted $MgII\lambda 2800$ profile that is significantly less broad ($\sim 20\%$) than $H\beta$ making it the virial estimator of choice. Pop. A $H\beta$ profiles are best fit with a single symmetric Lorentz function. Gaussian fits to Pop. A profiles will result in a systematic overestimation of M_{BH} . This paper focuses mainly on Pop. B sources where broader and more complex lines are observed. A subset of Pop. A sources show a significant $MgII\lambda 2800$ blueshift (Paper I) making FWHM $H\beta$ a safer virial estimator. These sources can be described as the youngest least-evolved quasars with strong ongoing star formation among

all quasars in the present sample (e.g., Mathur 2000; Sani et al. 2010; Sulentic et al. 2000a; Wang et al. 2006). Extreme values of R_{FeII} appear to be an empirical signature of quasar youth perhaps reflecting extreme low ionization and metal enrichment as well (c.f. Paper I).

The advent of the Sloan Digital Sky Survey (SDSS) makes possible accurate direct comparison of $H\beta$ and MgII λ 2800 using the brightest 600+ quasars where *both* lines appear in the spectra (§2 describes the sample of SDSS quasars). Individually most of these spectra are too noisy (typically $s/n < 5$ in the continuum near the two lines) to yield good measures and, therefore, a reliable application of M_{BH} –FWHM–relations. We want to move beyond single-epoch measures of the past 20 years involving random samples that yield the same result – quasar black hole masses with mean $M_{\text{BH}} \sim 8.5 \pm 1.5$ (see the paradoxical result of Croom 2011). We think that the best path to accomplish this goal involves generation of median composite spectra in the 4DE1 context (Sulentic et al. 2002, §3). The composites can provide very high s/n line profiles from which more accurate measures can be obtained. Results about line profiles and trends are given in §4. Our findings are discussed in §5 that presents the necessary cautions and calibration factors that can ultimately yield improved M_{BH} values. We will only briefly analyze (§5.5) a luminosity-dependent scaling law such as the one recently presented in Trakhtenbrot & Netzer (2012) as well as the determination of \mathcal{F} that is a distinct and very complex problem (e.g., Collin et al. 2006; Graham et al. 2011; Netzer & Marziani 2010; Park et al. 2012).

2. Sample Selection and Spectral Binning

2.1. Sample Selection

Spectral binning offers the possibility to generate much higher s/n composite spectra using the SDSS database if a binning context can be identified. We searched SDSS-DR7 for sources catalogued as type-1 AGN (quasars) in the redshift range 0.4 – 0.75 and with magnitudes brighter than ≈ 18.5 in the g , r or i bands. Below the assumed magnitude limit the low s/n of individual spectra make it difficult to estimate even FWHM $H\beta$ and R_{FeII} well enough to permit reliable bin assignments. We also searched the list of Zhou et al. (2006) in order to include type-1 AGN showing broad line FWHM $H\beta < 1000 \text{ km s}^{-1}$. Such sources are not identified as quasars in SDSS but show strong FeII emission characteristic of type 1 AGN. The resultant sample consisted of 716 quasars. The next step involved discarding very noisy spectra and some sources with unusually red colors (obviously reddened quasars where MgII λ 2800 was very weak or absent) thus reducing the sample (the same one considered in Paper I) to 680 quasars. Narrow and broad absorption line sources were excluded from the sample unless, in the case of narrow absorption lines, the absorption was judged insufficient to affect our ability to measure broad line binning parameters.

2.2. Spectral binning

Spectral binning in the 4DE1 optical plane maps sources using measures of FWHM $H\beta$ vs. $R_{\text{FeII}} = W(\text{FeII}\lambda 4570) / W(H\beta) \approx I(\text{FeII}\lambda 4570) / I(H\beta)$, where $H\beta$ refers to measures of the broad line profile of $H\beta$ ($H\beta_{\text{BC}}$) corrected for narrow line $H\beta$ emission as well as any contamination from [OIII] $\lambda\lambda 4959, 5007$, HeII $\lambda 4686$, and FeII emission (Sulentic et al. 2002). Recent works, including the present one consider the intensity ratio rather than the ratio of equivalent widths. Spectral types are defined by binning in intervals of R_{FeII} ($\Delta R_{\text{FeII}} = 0.5$, from A1 [$R_{\text{FeII}} < 0.5$] to A4 [$1.5 \leq R_{\text{FeII}} < 2.0$]) and FWHM ($\Delta \text{FWHM } H\beta = 4000 \text{ km s}^{-1}$, from A1 ($\text{FWHM } H\beta \leq 4000 \text{ km s}^{-1}$) and B1 to B1⁺⁺ [$12000 \text{ km s}^{-1} \leq \text{FWHM } H\beta < 16000 \text{ km s}^{-1}$]). Separation of the sample into spectral types will allow us to avoid the danger of mixing together sources that show very different spectral line profile

properties. Insofar as $H\beta$ and $FeII$ measures reflect physical conditions in the BLR, the bins isolate sources with similar values of density, ionization parameter, and L/L_{Edd} (see e.g., Marziani et al. 2010, 2001). Binning allows us to also take into account the complexity of line profiles and to separate, at least in an heuristic way, major flux contributions that are due to gas that is not likely to be virialized (i.e., the redshifted very broad component of $H\beta$ in Population B sources). Bin assignments were made as described in Paper I. We made a final inspection supplemented by IRAF SPLOT measures, for sources falling near bin boundaries. A few dozen sources were moved into adjacent bins but none of this fine tuning is likely to have had much effect on resultant median composites. Two bins (A2 and B1) are most densely populated while our binning contains enough sources to permit generation of composites for 8 bins that span the FWHM $H\beta$ and R_{FeII} ranges occupied by the majority of low redshift type 1 sources (with an inferred 2 dex range in Eddington ratio, $0.01 \lesssim \log L/L_{Edd} \lesssim 1$ that is the one of luminous type-1 AGN; Davis & Laor 2011; Kollmeier et al. 2006; Marziani et al. 2003b; Woo & Urry 2002).

Table 1 gives the number of sources (N_{tot}) in each bin. Boldface numbers indicate spectral types for which a composite spectrum was constructed. The separation into Pop. A and B sources divides almost evenly low redshift $z < 1.0$ quasar samples (45% Pop. B. in Zamfir et al. (2010) and 54% in this study). Bin B2 was almost devoid of sources in previous studies of low-luminosity sources (Marziani et al. 2003a; Zamfir et al. 2010) while it accounts for 3% of the present sample. Sources with B2 spectra are more numerous at high luminosity where they account for $\lesssim 20\%$ of our Very Large Telescope ISAAC sample (Marziani et al. 2009). Given the shape of the source distribution in the 4DE1 optical plane and the crudeness of the binning it is likely that bin A1 is a blend of A2 and B1 sources. The B2 composite is mainly due to spectra of sources whose location in the 4DE1 optical plane is close to the boundary of A2 and B1. In other words it could be that B2 sources are a physically diverse mixture (Marziani et al. 2001). More than anything else, B2 provides a hints of the confusing results that one would obtain mixing B1 and A2 spectra. Data and measures on B2 are reported but scantily discussed.

2.3. Radio-Loud Sub-Samples

The entire sample of 680 binned quasars was cross-correlated against the Faint Images of the Radio Sky at Twenty-Centimeters (FIRST) catalogue (Becker et al. 1995). Radio maps and catalogue data for 163 FIRST-detected sources were used to isolate radio-loud (RL) quasars from the general radio-quiet (RQ) population. The majority of RL sources belong to Pop. B (Sulentic et al. 2003; Zamfir et al. 2008). Most radio-detected RQ sources show core-dominated (CD), sometimes core-jet morphology. Sources were classified as RL lobe-dominated (LD) when a visual inspection revealed a complex, usually double-lobe structure. All sources except one¹ have radio power $\log P_\nu \geq 31.6$ at 1.4 GHz (P_ν in units of $\text{erg s}^{-1} \text{Hz}^{-1}$), the nominal lower specific power for Fanaroff-Riley II (FRII) sources. The radio morphology defines the classical RL phenomenon with the weakest FRII sources providing an empirical lower limit for this activity. Compact sources were considered core-dominated (CD) RL if their rest frame specific emission was above the FRII lower limit, as in Zamfir et al. (2008). This corresponds roughly to $R_K = 70$ as defined in Kellermann et al. (1989). The lower limit of radio power in FRII sources excludes all or most radio-detected RQ sources that appear as CD in FIRST. Table 1 reports the number of sources in each bin along with the numbers of FIRST detections (N_{FIRST}). FIRST non-detections (i.e. undetected RQ sources) and detections are tabulated in columns 3 and 4. FIRST should detect all RL sources in the redshift range under consideration. Radio detections

¹ SDSS J093704.05+293704.9 has $\log P_\nu \approx 31.2$ at 1.4 GHz but classical FRII morphology.

were assigned an FRII or CD morphology (numbers of sources are in columns 5 and 6) based on inspection of FIRST images.

3. Generation and Analysis of Composite Spectra

Three steps preceded generation of composite spectra: 1) assignment of sources to spectral bins as described in the previous section, 2) deredshifting of source spectra using SDSS z values, and 3) application of a second-order correction connected with a known bias in SDSS redshift estimates (Hewett & Wild 2010). Accurate rest frame definition can be a serious problem. Knowledge of the rest frame is important for identification and physical interpretation of internal broad and narrow line shifts that show a wide velocity range. They differ widely from source to source and depend on ionization state (Gaskell 1982; Tytler & Fan 1992). The technique used for redshift computation in SDSS is reliable but not accurate enough to yield uncertainties as low as $\approx 30 \text{ km s}^{-1}$ (Hewett & Wild 2010). The [OIII] $\lambda\lambda$ 4959,5007 line strength is a known E1 correlate with [OIII] $\lambda\lambda$ 4959,5007 becoming weaker, broader, and hence more difficult to measure as one proceeds from B to the A1 bin and along the sequence from bin A1 to A4 (Sulentic et al. 2002; Zamfir et al. 2010). Bin A3 and A4 sources show a systematic [OIII] $\lambda\lambda$ 4959,5007 blueshift with respect to low ionization narrow lines. The shift amplitude in these “blue outliers” is also believed to be related to the E1 sequence (Hu et al. 2008; Komossa et al. 2008; Marziani et al. 2003b; Zamanov et al. 2002).

Wavelengths of the three most prominent narrow lines [OII] λ 3727, $H\beta$, and [OIII] λ 5007 were measured whenever detected. Systematic shifts were computed taking an average of the three lines in each source spectrum and clipping individual measurements in cases of disagreement because of poor data or intrinsic blueshift of [OIII] λ 5007. This means that in several cases only two lines could be used for redshift determination. In a few cases (especially in A3 and A4 bins, where oxygen lines can be very weak) only $H\beta_{\text{NC}}$ could be used or, failing that, the adopted SDSS z value. The “bias” in the SDSS redshift determination is larger for extreme A bins but relatively small for Pop. B and bin A1 sources. This is not surprising, since bin B1 shows stronger and sharper narrow lines that permit more accurate redshift determinations with the SDSS algorithm.

After sample selection, bin assignments, and redshift correction we generated median composite spectra for $H\beta$ and MgII λ 2800. RL and RQ composites was also constructed for bin B1. Wavelength uncertainties of composite spectra were quantified by measuring a posteriori additional low-ionization narrow lines. Systematic effects were found to be small, with a radial velocity difference $\Delta v_r \lesssim 25 \text{ km s}^{-1}$. The dispersion in radial velocity is $\sigma_{\Delta v_r} \lesssim 50 \text{ km s}^{-1}$ for all bins in line with estimations of Hewett & Wild (2010). In practice this means that any line is assumed to be unshifted if $\sigma_{\Delta v_r} \lesssim 100 \text{ km s}^{-1}$.

3.1. $H\beta$ and MgII λ 2800 spectral range

Interpretation of the $H\beta$ and MgII λ 2800 spectral ranges closely follows previous work (Boroson & Green 1992; Marziani et al. 2003a) and has been discussed in Paper I. We only mention that emission blends near MgII λ 2800 are mainly due to FeII which is modeled with the FEII_{UV} emission template provided by the last model in Table 1 in Brühweiler & Verner (2008). Main results presented in this paper were also tested with an additional empirical template produced by Tsuzuki et al. (2006). FeI emission was detected in Paper I, but appears to be fainter (along with any contribution due to Balmer continuum) in B spectral types. Adopted ranges for the multicomponent fitting analysis are 2600 Å – 3050 Å and 2400–3100 Å for Pop. A and B respectively. Known non-iron lines in this region include [NeIV] 2423.8, [OII] 2471.0, semi-forbidden AlII] 2669.95, O III 2672.04, and most probably HeI 2945.11.

3.1.1. The ratio of the MgII λ 2800 lines

The intensity ratio of the MgII λ 2800 doublet $\mathbb{R} = I(\text{MgII}\lambda 2796.35) / I(\text{MgII}\lambda 2803.53)^2$ due to transitions $^2P_{3/2} \rightarrow ^2S_{1/2}$ should be 2:1 in the pure optically thin case. In the case of infinite optical depth the ratio should be 1:1 (i.e., if lines are fully thermalized). For intermediate conditions the ratio depends on electron density, temperature, and column density. Under standard assumptions the condition for thermalization on the product ionization parameter times hydrogen density n_{H} is $Un_{\text{H}} \gtrsim 1.7 \cdot 10^7 \text{ cm}^{-3}$ (Hamann et al. 1995; Laor et al. 1997). We therefore expect an \mathbb{R} value close to 1:1 for likely values of U and n_{H} in both the BLR and the very broad line region (VBLR) associated with the VBC. An array of CLOUDY (Ferland et al. 1998) simulations predicts the intensity ratio as a function of hydrogen density n_{H} and ionization parameter U (Fig. 1; a fixed hydrogen column density of 10^{24} cm^{-2} and solar abundances are assumed).

The individual lines are too broad and hence too blended to permit reliable direct measurement. A-priori values must be assumed for BC and VBC (the latter only for Pop. B sources) and the values could be different *in lieu* of the different physical conditions expected for the BLR and the VBLR (Marziani et al. 2010). In the BLR, $\log U = -2.75$, $\log n_{\text{H}} = 12.50$ yield $\mathbb{R} \approx 1.3:1$. The observed ratio \mathbb{R} in a typical Population A NLSy1 source (I Zw 1) is 1.2. We assume a *standard* value of 1.25, noting that a small change of ± 0.05 in the doublet ratio does not affect line decomposition and FWHM measurement.

The intensity of MgII λ 2800 is difficult to compute by photoionization codes because the line is primarily emitted in the partially ionized zone, where a local approximation (i.e., via a local mean escape probability) treatment of radiation transfer is probably inadequate. It is possible that the MgII λ 2800 lines become fully thermalized at the extreme optical depth of the LIL emitting part of the BLR, justifying the assumptions of a 1:1 ratio. In the following we have therefore considered both cases. Mock MgII λ 2800 profiles were computed for 1:25 and 1:1 cases assuming a wide range of line FWHM. The peak wavelengths used as a reference whenever the doublet is treated as unresolved, are 2800.1 Å and 2799.4 Å for the 1:1, 1.25:1 cases respectively. These values are found to be almost independent of FWHM. We assumed that the doublet wavelength cannot be shorter than 2799.1 Å, the value obtained for the case $\mathbb{R} = 1.5:1$. Values of $\mathbb{R} \gtrsim 1.5$ are unlikely for the physical conditions expected within the BLR (Fig. 1).

In the VBLR, $\mathbb{R} \approx 1.5$ is appropriate for $-1 \lesssim \log U \lesssim -0.5$ and for high density values ($n_{\text{H}} \gtrsim 10^{11} \text{ cm}^{-3}$), and only values $\mathbb{R} \gtrsim 1.7$ are unlikely. Considering however that the doublet component separation is $\Delta\lambda \approx 8 \text{ Å} \ll \text{FWHM}(\text{VBC})$, the VBC can be treated as a single line. Under this assumption the doublet ratio is indeterminate.

4. Results

4.1. Broad Line Profile Shapes

Composite spectra for Pop. B sources are shown in Fig. 2, and Fig. 3, after continuum subtraction (Pop. A median spectra were shown in Paper I). Table 2 reports FWHM, asymmetry index A.I., kurtosis κ and centroid at fractional intensity measures for the H β and MgII λ 2800 broad profiles (i.e. after narrow components and FeII subtraction but before broad/very broad component decomposition) of both Pop. A and B spectral types. A.I., κ and centroids are defined by Eqs. 1 – 3 in Zamfir et al. (2010). Note that A.I. is defined at $\frac{1}{4}$ maximum intensity and with respect to line peak while centroids are relative to source rest frame. These parameter values provide an empirical description of the profile without any model assumption. Reported uncertainties are at 2σ confidence level and have been

² In this paper vacuum wavelengths are used. Line identification includes the optical wavelength of traditional use. For example, we refer to [OIII] λ 5007 even if the reference wavelength is 5008.2 Å.

computed measuring the effect on the profile parameters of changes in continuum placement (always less than 2%, due to the extremely high s/n). Note that full profile measures for MgII λ 2800 doublet assumed an unresolved single line. Width measures for MgII λ 2800 can be converted to single component width by subtracting 300 km s^{-1} (Trakhtenbrot & Netzer 2012). Zero point wavelengths set by [OII] λ 3727 and H β narrow component agree within an rms of 10 km s^{-1} . Uncertainties were estimated by propagating the zero point rms, the scatter associated with SDSS wavelength calibration and the uncertainty of continuum placement.

The most important results from Table 2 are the difference in line profile properties for Pop. A and B. FWHM differences among Pop. B spectral types arise from the definition of 4DE1 and how it is binned. Pop. A sources show broader, more symmetric and less shifted H β profiles than MgII λ 2800 with the exception of bins A3 and A4 where a blue asymmetry is observed. MgII λ 2800 and H β both show a symmetric unshifted profile in bins A1 and A2. The broad MgII λ 2800 profile appears symmetric but blueshifted by $\approx -300 \text{ km s}^{-1}$ in bins A3 and A4 and these are the only sources where FWHM MgII λ 2800 exceeds FWHM H β . This has been seen before and interpreted as evidence for outflows in the highest L/L_{Edd} A3 and A4 sources (Paper I), possibly because of a distinct LIL component connected to the blue shift observed in HILs like CIV λ 1549.

Pop. B sources are largely represented by bins B1 and B1⁺. Figure 2 confirms previous claims (Wang et al. 2009) that FWHM H β is systematically broader than FWHM MgII λ 2800 by approximately 20%. This appears to be true for all B bins as well as bins A1 and A2. Both H β and MgII λ 2800 Pop. B profiles show median red asymmetries; MgII λ 2800 show perhaps slightly weaker asymmetries. Centroid shifts are redward and of larger amplitude in H β than MgII λ 2800. The red asymmetry in the lower half of the profile was previously interpreted, in the case of H β , as a signature of the VBC (Sulentic et al. 2002, 2000c). Apparently MgII λ 2800 shows a (weaker) VBC component. Much of the excess H β profile width may be due to a stronger VBC component. In other words, the measures on line profiles of Pop. B reported in Tab. 2 suggest that H β is more strongly affected than MgII λ 2800 by non-virial motions especially toward the line base. However, the VBC cannot be a full explanation for the difference in line width between MgII λ 2800 and H β because A1 and A2 (where no VBC is present) show the same effect.

Somewhat higher kurtosis values are found for broader Pop. B sources since Pop. A profiles are more sharply peaked (c.f. Kollatschny & Zetzl 2013, see §5.3 for interpretation). The kurtosis index is consistent with a single Gaussian profile ($\kappa \approx 0.44$) only for spectral type B1⁺⁺ for both H β and MgII λ 2800. B1⁺⁺ profiles are rare, very broad and complex sometimes showing double peaked lines although not in our sample.

4.2. Multicomponent Analysis

IRAF SPECFIT (Kriss 1994) was used to model and decompose line blends and components in Pop. B composites as previously reported for Pop. A composites (Paper I). We assumed a weak MgII λ 2800 narrow component in Pop. B composites (see Wang et al. 2009 and references therein) constrained to not exceed the ratio MgII λ 2800/H $\beta_{\text{NC}} \approx 2$ (appropriate for $\log U \sim -2$ and $\log n_{\text{H}} \approx 4 - 5$). A double Gaussian model involving an unshifted BC and redshifted VBC was used for fits to both lines following previous work on H β (Marziani et al. 2009; Fig. 2, and Fig. 3). In contrast to Pop. B, the majority of Pop. A profiles were well fit by an (almost) unshifted symmetric Lorentz function. Table 3 presents BC and VBC measures (intensity, peak shift and FWHM) for H β and MgII λ 2800 for B spectral type and for the source PG 1201+436. Uncertainties are 2σ confidence level. Uncertainties of peak shifts were computed by quadratically propagating errors on zero point, wavelength calibration rms and uncertainty provided by the fitting routine

(Paper I). Uncertainties reported for the VBC should be considered as formal errors and are computed following the assumption that the best fit is the correct one and that the functional form describing the line component is also correct. The VBC is a broad component with poorly constrained centroid and width. More realistic uncertainties are estimated around 20% for both shift and width measures.

Our operating assumption is that unobscured gas in virial motion should give rise to a reasonably symmetric/unshifted line profile. The BC component is therefore the virial estimator that we are trying to isolate. The use of a double Gaussian model in SPECIFY was motivated by the inflected appearance of the $H\beta$ profile (this is evident in the B1 panel of Fig. 2). Decomposition of the BC/VBC blend was the most uncertain part of the modeling. We derive the ratio of BC / VBC intensity for the two lines from the fit in the B1, B2 and B1⁺ cases. However, we do not know the shapes of the individual components. A highly redshifted VBC is unlikely to show a symmetric Gaussian profile. Past work has focussed on $H\beta$ and has used very high s/n composites like the ones presented here. Past work involving BC+VBC decomposition (Marziani et al. 2009; Sulentic et al. 2002) is limited and shows FWHM $H\beta$ BC and shift values in the range 4000-4800 km s⁻¹ and zero km s⁻¹, respectively, with the relative strength of the VBC possibly increasing with source luminosity.

Modelling is clearly more ambiguous in sources with broader multicomponent profiles. The MgII λ 2800 profile in Pop. B sources also deviates from a single Gaussian showing a narrower core and more prominent wings. In other words it is more similar to a Lorentz/Voigt profile that can be approximated by the sum of the Gaussians. An attempt to fit MgII λ 2800 in the B1 composite with a single Lorentzian will reproduce the observed red wing but model the blue one with a significant excess. The sum of two Gaussians, with the broadest one slightly redshifted provides a satisfactory fit (Fig. 2). The introduction of a small shift in the broader Gaussian accounts for the excess flux in the red wing, prominent in $H\beta$ but also detected in MgII λ 2800. Nonetheless the assumption that the VBC is a shifted symmetric Gaussian is unlikely to be correct for such a redshifted component: non-virial motions are likely to strongly affect the VBC. We currently have no empirical basis for fitting the VBC with more complex models. Our best current fits suggest that the MgII λ 2800/ $H\beta$ intensity ratio differs for the VBC and BC: with MgII λ 2800/ $H\beta$ \gtrsim 1.5 for the BC and MgII λ 2800/ $H\beta$ \lesssim 1 for the VBC. This result is consistent with the idea that the VBC arises in a higher-ionization VBLR near the inner edge of the BLR (Korista & Goad 2004).

Modeling the VBC as a distinct component is further justified by the discovery of sources where the $H\beta$ profile is dominated by the VBC with little or no detected BC (e.g. PG 1416-129 in Sulentic et al. (2000c) and 3C110 in Marziani et al. (2010)). In the course of assembling the sample under consideration in this study we found a few more VBC dominated sources. The best example involves PG 1201+436 whose $H\beta$ and MgII λ 2800 profiles are shown in Fig. 4. Most of the broad redshifted $H\beta$ profile is almost certainly VBC with little or no BC emission. The most straightforward interpretation of the MgII λ 2800 profile is, conversely, BC dominated with much weaker VBC emission. We can use these considerations to cautiously guide SPECIFY in modelling of MgII λ 2800 in bin B sources with the broadest profiles i.e., B1⁺⁺. B1⁺⁺ sources however constitute less than 3% of our sample. They are however relevant if for no other reason that bin B1⁺⁺ shows the largest RL fraction in the 4DE1 sequence (Zamfir et al. 2008 and Tab. 1). This is also the domain of some of the best known sources that show double-peaked profiles (Eracleous & Halpern 2003) although most do not. A BC+VBC profile with peaks near zero + redshift is not a double peaked profile. The fit for B1⁺⁺ shown in Figure 3 assumes a BC-dominated MgII λ 2800 profile and attempts to maximize MgII λ 2800 BC intensity and

width. It is interesting that the resulting MgII λ 2800 profile: 1) remains less broad than H β _{BC} and 2) requires a VBC component to produce an acceptable fit.

Results detailed in Table 3 and Figures 2 + 3 indicate that in Pop. B sources MgII λ 2800 mimics H β by showing a VBC component. They also show that the VBC has a stronger effect on FWHM H β when measuring the full profile. In this sense FWHM MgII λ 2800 BC appears as a safer virial estimator than FWHM H β . BC measures are preferred as virial estimators for both lines with a consistency correction factor taking into account the fact that FWHM MgII λ 2800 (BC) is 20% narrower than FWHM H β for the majority of sources (B bins and bins A1+A2, 90 % of our sample). Nonetheless, all measures reported in Tab. 2 and Table 3 for all spectral types excluding A3 and A4 show that the FWHM of *any* MgII λ 2800 component is narrower than the equivalent H β component. This result is robust since it also holds for the full profile.

Tab. 3 indicates that B1 sources may show a significant MgII λ 2800 BC blueshift, with smaller amplitude in km s⁻¹ than the one measured in Pop. A. A small blueshift might also be present for B1⁺⁺. Part of the BC blueshift might result from modeling the VBC with a symmetric profile and possibly over-subtracting flux from the red side of the BC. It is however unlikely that this accounts for the full effect since a blueshift is also measured for the full profile: a blue-side excess is visible in the median B1 MgII λ 2800 profile shown in Fig. 2. Tab. 2 indicates a MgII λ 2800 blueshift for spectral types B1 and B2 with any blueshift in B1⁺⁺ BC not detected by our parameterization of the full profile. The relevance of the blue shifts in Pop. B profiles will be further discussed in §4.4 and §5.

4.3. Radio Loud

RL sources, both CD and FRII (Fig. 5) B1 medians show a symmetric (FRII) or redshifted (CD) MgII λ 2800 line core. The profiles resembles the typical B1 RQ and full sample profiles but there is no hint of possible blue shifts. A shift to the red is observed at 1/4 intensity level but, again, the shift amplitude is less than for H β . The redward asymmetry is especially prominent in CD sources with a $\frac{1}{4}$ centroid displacement reaching 600 km s⁻¹. CD and FRII sources do not show any large difference in FWHM since they were both chosen to belong to spectral type B1 by imposing the same condition on FWHM H β . Their interpretation will be discussed in §5.4.

4.4. Major trends

We focus on line shifts and widths because they are parameters relevant to the credibility/definition of a virial broadening estimator. Comparison of centroid shift values at different heights in a line give the best way to evaluate asymmetry and line shift. The behavior of Pop. B is different than Pop. A showing a redshift that is strongest in the line base resulting in red asymmetric profiles. We assume that modeling and subtraction of a VBC component will enable us to measure the width of a symmetric and unshifted BC virial estimator. Pop A sources in bins A1 and A2 yield a FWHM measure requiring no VBC correction. A correction is needed only to make consistent virial estimate using FWHM H β and FWHM MgII λ 2800. In bins A3 and A4 the FWHM H β measure is preferred after correction for a blue asymmetry.

Rather than the amplitude in km s⁻¹, a value normalized by line width provides a more direct evaluation of the “dynamical relevance” of any line shift. We can define the following parameters

$$\delta\left(\frac{i}{4}\right) = \frac{c\left(\frac{i}{4}\right)}{\text{FWHM}_i}, i = 1, 2, 3, \quad (2)$$

where the centroid $c(\frac{i}{4})$ at fractional peak intensity $\frac{i}{4}$ has been normalized by the full width at the same fractional peak intensity $\text{FW}\frac{i}{4}\text{M}$. Fig. 6 shows the behavior of $\delta(\frac{3}{4})$ and of $\delta(\frac{1}{4})$ as a function of spectral type (error bars are obtained propagating quadratically the uncertainties in Table. 2). A radial velocity v_r shift close to a line peak may represent a systematic effect involving the entire emitting region only if it is also seen at $\frac{1}{2}$ and $\frac{1}{4}$ fractional intensities. Fig. 6 confirms that the B1 $\text{MgII}\lambda 2800$ blueshift is much less relevant than shifts found in bins A3 and A4. We also note that in bin A3 and A4 the shift measured for the full $\text{MgII}\lambda 2800$ profile is probably a lower limit, since the profile can be interpreted as the sum of an unshifted line + a blueshifted component (§3.3 of Paper I). The line base might be affected by the presence of additional kinematic components that, in our interpretation of the line profiles, are the blueshifted component (blue in Marziani et al. 2010) and the VBC for Pop. A and B respectively. Considering the $\frac{1}{4}$ centroids as a function of spectral type, only bins A3 and A4 show a relatively large $\text{H}\beta$ blueshift (the peaks are almost unshifted). Bin A1 and A2 show symmetric profiles in both $\text{H}\beta$ and $\text{MgII}\lambda 2800$. The situation changes in Pop. B where the B1 and B1^+ $\text{H}\beta$ profiles are strongly red asymmetric with the B1^+ centroid shift reaching $\approx 800 \text{ km s}^{-1}$. Conversely the $\text{MgII}\lambda 2800$ profile shows a more symmetric shape. There is a significant shift at $\frac{1}{4}$ intensity level but its amplitude is ~ 0.25 that of $\text{H}\beta$. Given the large $\text{FW}\frac{1}{4}\text{M}$ for $\text{MgII}\lambda 2800$, the δ values are lower than in the case of $\text{H}\beta$. Similar considerations apply to $\frac{1}{2}$ intensity – the line intensity level at which the virial broadening is computed: $\text{MgII}\lambda 2800$ shows modest amplitude normalized shifts (Fig. 7).

Eddington ratio estimates are needed to infer the physical meaning of differences between A and B spectral types. We computed the median mass from the medians of the fluxes of individual sources in each bin and from FWHM measured on the median composite. We follow the prescriptions of Assef et al. (2011) and Shen & Liu (2012) to compute M_{BH} from $\text{H}\beta$ and $\text{MgII}\lambda 2800$ line widths respectively. Trends are preserved also with older relations linking the black hole mass to the FWHM and the continuum at 3100 or 5100 Å. The bolometric luminosity needed for L/L_{Edd} has been derived from the luminosity at 5100 Å following Nemmen & Brotherton (2010). Values of bolometric luminosity, M_{BH} and L/L_{Edd} computed using the BC as a virial broadening estimator are reported in the first columns Table 4, followed by M_{BH} and L/L_{Edd} computations using the whole profile (treating $\text{MgII}\lambda 2800$ as a single line). M_{BH} values derived from BC and presented in Table 4 show a trend toward decreasing M_{BH} from A1 to A4. A constant median L in the bins ($\log L \sim 46.0$) implies a trend of increasing L/L_{Edd} from A1 to A4. We do not see this trend if we use $\text{MgII}\lambda 2800$ measures reflecting the absence of a clear correlation between $\text{H}\beta$ and $\text{MgII}\lambda 2800$ line profile measures in Pop. A. Pop. B sources show a more regular behavior preserving a trend. This is mainly due to the definition of B spectral types based on increasing line width. However, inclusion of VBC leads to an overestimate of $\log M_{\text{BH}}$ for both $\text{H}\beta$ and $\text{MgII}\lambda 2800$ derived masses.

Fig. 7 shows the behavior of $\delta(\frac{1}{2})$ and of the FWHM ratio between the broad component of $\text{MgII}\lambda 2800$ and $\text{H}\beta$ as a function of Eddington ratio since the E1 sequence is mainly a sequence of L/L_{Edd} .³ The parameter $\delta(\frac{1}{2})$ is considered as an appropriate indicator of the dynamical relevance of the shift because FWHM is a virial broadening estimator of choice. The δ trends at $\frac{1}{4}$ and $\frac{3}{4}$ peak intensity as a function of spectral type are preserved also as a function of L/L_{Edd} and are not shown again. The $\text{MgII}\lambda 2800$ blueshift starts increasing at $\log L/L_{\text{Edd}} \sim -0.6$, as the A3 and A4 sources behave differently from all other sources,

³ Our sample bins have median L_{bol} that is almost constant. This follows from the flux and redshift limits of our sample, and implies that for any trend as function of L/L_{Edd} , there is a corresponding trend with M_{BH} . M_{BH} is a one-way estimator of a quasar evolutionary status. However, the presence of line shifts is more probably associated to the relative balance of gravitation and radiation forces so that we will assume in the following that the relevant physical parameter is L/L_{Edd} .

as discussed in Paper I. The marginal blueshift detected at $\frac{3}{4}$ maximum for spectral type B1 becomes untraceable at $\frac{1}{2}$ intensity. At $\frac{1}{2}$ maximum the MgII λ 2800 profile is mostly unperturbed in all B bins (save B2 that includes a tiny minority of sources and is probably a confusing mixup), while the H β profile shows a highly significant shift to the red.

5. Discussion

5.1. MgII λ 2800 and H β in the Pop. A and B Context

Virial estimates of M_{BH} for large quasar samples have been available now for more than 10 years (e.g. McLure & Dunlop 2004; McLure & Jarvis 2002). Estimated masses lie within the range $\log M_{\text{BH}} \sim 6.0 - 11.0$ with uncertainties in the range 0.2–0.4 dex at 1σ confidence. The latter uncertainty value appears more realistic when different estimates for the same sources are compared. This is also confirmed when we compare different mean mass estimates for quasar populations (e.g. radio-quiet vs. radio-loud). This situation has led to claims that FWHM measures contain little or no information about black hole mass (Croom 2011) and others arguing that FWHM measures for different lines are equally valid M_{BH} estimators (Vestergaard et al. 2011). We argue that neither of these claims is valid and that the path to a clearer picture lies within the concept of a quasar parameter space like 4DE1. Quasars do not distribute randomly in 4DE1.

How can we move towards more accurate and consistent M_{BH} estimates for individual quasars and quasar populations? It is unlikely that inconsistencies are due only to comparisons involving spectra of different s/n (Assef et al. 2012). Inconsistencies remain when comparing estimates using the same (i.e. SDSS) spectra. The s/n is certainly an issue but its effect depends upon the structure of the line profiles used as virial estimators (see e.g. Shen et al. 2008, 2011). Lines well-fit with single unshifted components are likely the most robust in the face of declining s/n. However many broad lines in type 1 AGN show line shifts and asymmetries while others are obviously not well fit with a single component. Fitting lines with a single Gaussian is inappropriate because the profile shapes are rarely well approximated by a single Gaussian. For example, an attempt to fit the MgII λ 2800 line of spectral type B1 with a single Gaussian would lead to a (bad) fit resulting in an overestimation of FWHM by 700 km s^{-1} . Effects of erroneous assumptions on fitting function depend on s/n in a way that depends on the intrinsic shape and on noise properties. Composites spectra have very high s/n and allow one to focus on systematic effects with minimal measurement (statistical) errors. The challenge is to generate composites in a clear and unbiased way which means binning physically similar quasars.

If any broad lines serve as virial estimators then MgII λ 2800 and H β are the safest choices. Results presented in this paper suggest that MgII λ 2800 is the line least affected by profile shifts and asymmetries in 90% of all quasars. We maintain that a first step in the path to progress requires recognition that quasars showing $\text{FWHM H}\beta < \text{or } > 4000 \text{ km s}^{-1}$ (Population A and B respectively) have very different profile properties (Collin et al. 2006; Sulentic et al. 2000b; Zamfir et al. 2010). In other words, the dispersion in estimated M_{BH} and resultant L_{Edd} measures is not found by luminosity binning (at fixed z) but rather by binning in the 4DE1 context that reflects differences in BLR kinematics and geometry.

Figure 8 (left) overlays our composite measures of FWHM H β vs. FWHM MgII λ 2800 (with the MgII λ 2800 doublet treated as a single line) on the individual source measures from Wang et al. (2009). Full profile measures follow the source distribution and the best-fit regression of Wang et al. (2009). The large scatter at the low FWHM end and the convergence of the regression towards parity reflect the unusual behavior of sources in bins A3 and A4 where the FWHM offset between H β and MgII λ 2800 breaks down. The convergence is also affected at the high FWHM end where the prominence of the VBC component increases in H β more than in MgII λ 2800. Figure 8 (right panel) presents our

BC values (all Pop. B sources corrected for the VBC) along with the parity line, the Wang et al. (2009) regression and our best fit to the median composite values. The main result is that we find no convergence but rather a constant offset ($\text{MgII}\lambda 2800 \approx 20\%$ narrower) from bin A2 through all B bins.

5.2. Implications for M_{BH} estimates of quasars: a tentative recipe

The previous analysis suggests the following recipe.

- 1 Identify a source as Population A or B – on the basis of $\text{FWHM H}\beta < \text{or} > 4000 \text{ km s}^{-1}$ respectively.
- 2a Bin A3 and A4 $\text{MgII}\lambda 2800$ profiles are unsuitable as virial estimators. Bin A3 and A4 $\text{H}\beta$ profiles are suitable if corrected for strong FeII contamination and for a blue component.
- 2b A1 and A2. Both $\text{H}\beta$ and $\text{MgII}\lambda 2800$ can be used as estimators without any correction.
- 3 Pop. B. Apply correction because of VBC to both $\text{H}\beta$ and $\text{MgII}\lambda 2800$, as described below.

A correction factor can be defined as the ratio between observed FWHM and BC FWHM:

$$\text{FWHM}(\text{line})_{\text{vir}} = \xi \text{FWHM}(\text{line})_{\text{obs}} \quad (3)$$

where

$$\xi = \frac{\text{FWHM}(\text{line})_{\text{BC}}}{\text{FWHM}(\text{line})_{\text{obs}}}, \quad (4)$$

and $\text{FWHM}(\text{line})_{\text{obs}}$ is measured on the whole profile (treating the $\text{MgII}\lambda 2800$ doublet as a single line). If a single-epoch FWHM measurement is made without consideration of the intrinsic shape then ξ is as reported in Tab. 5 (ξ values are derived from Tab. 3 and Tab. 2). The ξ factor is less important for $\text{MgII}\lambda 2800$ because the VBC component is always weaker. In the case of $\text{MgII}\lambda 2800$ a suitable ξ value is ≈ 0.85 . Table 5 indicates that a simple correction factor $\xi \approx 0.75 - 0.8$ could be applied to $\text{H}\beta$ once the object is classified as Pop. B, as suggested by Fig. 8. A simulation degrading the B1 spectrum with a combination of Gaussian and Poissonian noise shows that it is possible to recover a basic estimate of FWHM (with heavy smoothing) down to $\text{s/n} \approx 3$ (c.f. Shen et al. 2008, 2011), even if information on profile shape is completely lost. We also note that the ξ correction may be accurate excluding the most luminous sources where the VBC is extremely strong i.e., for $L_{\text{bol}} \gtrsim 10^{47} \text{ ergs s}^{-1}$ (Marziani et al. 2009), or the profile is not too irregular as it is the case of several sources in B1^{++} . The third column of Tab. 5 lists the multiplicative factor needed to convert from observed FWHM $\text{H}\beta$ to FWHM $\text{MgII}\lambda 2800$ BC. The last column lists the factor needed to convert the observed $\text{MgII}\lambda 2800$ FWHM into FWHM $\text{H}\beta_{\text{BC}}$.

The recipe reported above accounts for our result that the difference between $\text{MgII}\lambda 2800$ and $\text{H}\beta$ M_{BH} is positive at large L/L_{Edd} , and negative toward the lower end of the L/L_{Edd} distribution. If no correction is applied then $\text{MgII}\lambda 2800$ will be measured broader than $\text{H}\beta$ toward high L/L_{Edd} values (20% in A3 and $\approx 50\%$ in bin A4). Therefore at high L/L_{Edd} the $\text{MgII}\lambda 2800$ masses will be overestimated with respect to $\text{H}\beta$ which should actually provide a more reliable estimate. At low L/L_{Edd} the effect of the VBC on FWHM $\text{H}\beta$ is stronger yielding an M_{BH} estimate larger than the one from $\text{MgII}\lambda 2800$. The agreement with Fig. 1 of Onken & Kollmeier (2008) is quantitative (if rare outlying points in their Fig. 1 are excluded; medians by definition give no or low weight to extremes in a distribution):

$\Delta \log M_{\text{BH}} = \log M_{\text{BH}}(\text{MgII}\lambda 2800) - \log M_{\text{BH}}(\text{H}\beta) \approx 0.4$ dex for bin A4 with $\log L/L_{\text{Edd}} \approx -0.2$, and $\Delta \log M_{\text{BH}} \approx -0.4$ at $\log L/L_{\text{Edd}} \approx -1.7$.

Even if A3 and A4 represent only $\approx 10\%$ of our low redshift sample, high L/L_{Edd} are discovered with increasing frequency in high- z , flux limited samples. A recent study for $z < 1.8$ sources involving MgII λ 2800 and H α finds a small offset in the M_{BH} estimates, in the sense that MgII λ 2800-derived masses are slightly larger with respect to those from H β (Matsuoka et al. 2013). This might indicate an increasing frequency of MgII λ 2800 profiles affected by non-virial, outflow motions.

5.3. Origin of MgII λ 2800 emission and profile blue shifts

A major result of this paper is that FWHM MgII λ 2800 is systematically narrower than FWHM H β , excluding types A3 and A4. This holds for the full profile as well as for *all* the components identified in the lines: i.e. BC, VBC, blueshifted component. The simplest explanation is that MgII λ 2800 is emitted at larger radius, on average, than H β assuming that the gas is photoionized by a central continuum source. The emissivity Σ of the two lines was computed as a function of the ionization parameter U using CLOUDY simulations described in §3.1.1. The dependence on U was then converted to radial distance assuming a constant column density $\log n_{\text{H}} = 11$ [cm $^{-3}$]. If we approximate Σ with a power-law then $\Sigma \propto r^{-\alpha}$ yields $\Sigma(\text{MgII}\lambda 2800) \propto r^{-0.1}$ with a steeper trend for H β , $\Sigma(\text{H}\beta) \propto r^{-0.4}$, if $\log U \lesssim -0.5$. Elementary considerations suggest that the different emissivity law can lead to a different shape in the line wings and hence to a different FWHM for the two lines. The energy emitted in the line at distance r can be written as $E(r)dr = 4\pi r^2 \Sigma(r) f_c(r) dr$, where f_c is the covering factor. Since the virial assumption implies that $r \propto \frac{1}{v^2}$ the specific energy emitted per unit radial velocity is $E(v)dv \propto v^{-4} v^{2\alpha} f_c(v) \frac{dv}{v^3} \propto v^{2(\alpha-q)-3} dv$ if $f_c(r) \propto r^{-2+q}$. For $\alpha = 0.5$ and $q = 0$, $E(v) \propto v^{-2}$ which is the same general power-law describing Lorentzian line wings. A flatter emissivity law will yield a more peaked profile. Using the emissivity laws for MgII λ 2800 and H β , a 20% width ratio is obtained for reasonable values of q ($-\frac{2}{3} \lesssim q \lesssim \frac{1}{3}$, c.f. Netzer 1990). A more refined scenario involves the computation of the line profile following a weak-field approximation (Chen et al. 1989; Sulentic et al. 1998). Using the CLOUDY-computed emissivity laws for H β and MgII λ 2800, the profile of MgII λ 2800 turns out to be systematically narrower than H β by $\gtrsim 10\%$. The width ratio can be $\approx 20\%$ if the inner radius of the emitting disk is ≈ 250 gravitational radii. Therefore, the line width ratio and the Lorentzian-like profile shape can be explained in the context of virialized gas motions.

The MgII λ 2800 blueshift is most straightforwardly attributed to outflow of the line emitting gas with preferential obscuration of the receding part of the flow Paper I. A blueshift is suspected in the B1 composite (Fig. 2) but is not significant at a 2σ confidence level. The small amplitude of the shifts does not rule out a change in the intrinsic multiplet ratio as an alternative explanation in Pop. B sources: a value $\mathbb{R} = 2$ would yield an effective wavelength close to the one of the $^2P_{\frac{3}{2}} \rightarrow ^2S_{\frac{1}{2}}$ transition, 2796.35. If the effective wavelength is close to this value, then any systematic blueshift $\lesssim 300 \text{ km s}^{-1}$ will become insignificant. If the blueshift is associated with a low-density high-ionization component then a value as large as $\mathbb{R} \approx 1.7$ could be possible. However, the absence of any blueshift in bin A1 that is the simplest profile to analyze (1 component, weak FeII) argues against this suggestion.

Outflows driven by line or ionizing photon pressure can accelerate the line-emitting gas to a terminal velocity that is inversely proportional to the square root of the column density N_{c} and directly proportional to the Eddington ratio i.e.,

$$v_{\text{t}} \propto \left(\frac{1}{N_{\text{c}}} \frac{L}{L_{\text{Edd}}} \right)^{\frac{1}{2}} v_{\text{Kepl}} \quad (5)$$

where v_{Kep1} is the Keplerian velocity at the outflow starting radius.

If real the modest shift observed in the median spectra of B1 and B1⁺⁺ could be interpreted as the terminal velocity of a radiation driven outflow. This shift could occur even if $L/L_{\text{Edd}} \sim 0.01$ in gas with moderate column density $N_c \sim 10^{23} \text{cm}^{-2}$ (provided that the gas remains optically thick to the ionising continuum) that may in turn support the idea that resonant lines are driving, at least in part, the acceleration of the outflow (Ganguly et al. 2007; Proga et al. 2000; Sulentic et al. 2007). There is an intriguing similarity in the MgII λ 2800 and CIV λ 1549 behavior that may be related to the resonant nature of both lines but the effects on MgII λ 2800 appear by far less relevant than on CIV λ 1549 since the median MgII λ 2800 profile retains an overall symmetric appearance. The B1 and B1⁺⁺ profiles are *on average* only slightly perturbed by blueshifted emission: low- N_c gas might produce some scatter among B sources since it is most strongly affected by radiative forces and may become unbound following a continuum luminosity increase (Netzer & Marziani 2010). B1⁺⁺ sources are likely to be some of the lowest L/L_{Edd} sources. They are unstable in continuum emission and often show strongly variable emission line profiles with irregular shapes (Lewis et al. 2010). They are also rare ($\lesssim 3\%$ in the present sample) and are interpreted as the most evolved, perhaps dying or starving quasars in the 4DE1 sequence. An example involves the well-studied FRII source 3C 390.3 which belongs to bin B1⁺⁺ with line profiles characterized by a prominent blueshifted peak that produces a significant net profile blueshift. Another example with extreme velocity offset and large FWHM involves SDSS 0956+5128 (Steinhardt et al. 2012). Even if the interpretation of 3C 390.3 is currently a subject of debate (e.g. Dietrich et al. 2012; Zhang 2011), an application of the method of Negrete et al. (2012) indicates relatively low-density and high-ionization consistent with the overall properties of the blueshifted component identified in the spectra of many quasars (Marziani et al. 2010). A significant fraction of B1⁺⁺ sources in the present sample indeed show MgII λ 2800 profiles with large blueshifts/blueward asymmetries. Therefore, the marginal blueshifts of spectral type B1⁺⁺ median composite may reflect the somewhat erratic nature of low-density outflowing gas detected in sources whose unstable accretion rate may induce significant continuum fluctuations.

The high s/n of our composite spectra reveals a semi-broad component in the [OIII] $\lambda\lambda$ 4959,5007 profiles and on the blue side of H β_{NC} . B1 offers the most striking case along with PG 1201+436. In the B1 H β composite spectrum the excess flux is explained as a semi-broad component with width and shift similar to the [OIII] $\lambda\lambda$ 4959,5007 semi-broad component. That feature does not belong to the broad profile and would induce a blueshift of $\sim -100 \text{ km s}^{-1}$ into the BC model or into the measures of the broad line profile if not adequately taken into account. A similar interpretation is also possible for the small blueshifted “bump” observed in the H β and MgII λ 2800 profiles of PG 1201+436 (blue line in Fig. 4). The bump is modeled with a Gaussian component of width $1500 - 2500 \text{ km s}^{-1}$ and shift $-1500 - -2000 \text{ km s}^{-1}$. The inferred velocities and widths appear rather extreme to other cases where a semi-broad component of [OIII] $\lambda\lambda$ 4959,5007 is isolated. We can speculate that also this source is showing outflow largely in a region that might be at the boundary between the BLR and the narrow-line region (Zamanov et al. 2002). A more refined analysis of PG 1201+436 is deferred to later work (Sulentic et al., in preparation).

5.4. Radio quiet and radio loud

Core-dominated and lobe-dominated sources show a fairly symmetric profile, with evidence of a redshifted base due to the VBC that is especially prominent in CD sources (e.g., Punsly & Zhang 2011). The red excess is clearly detected also in MgII λ 2800 (a very convincing case is provided by the blazar 3C 279, Punsly 2013) although the A.I. is significantly lower than H β . The absence of any hint of blueshifts in RL profiles could be related to the

full suppression of an accretion disk wind, or it could be due to orientation. B1 bin was defined on a limited range of line width. Therefore we cannot expect to see the systematic FWHM difference mentioned above. In addition the fraction of FRII increases toward bin B1⁺⁺ i.e., broader sources. In bin B1 we are probably considering a subsample of FRII that show narrower profile than the majority of the population. If the FWHM is affected by orientation as expected (e.g., Rokaki et al. 2003; Runnoe et al. 2012; Sulentic et al. 2003; Wills & Browne 1986; Zamfir et al. 2008), we are observing sources that tend to be seen at smaller viewing angle than the general FRII population. If the wind flow follows a bent path over the accretion disk (Elvis 2000) or if the flow is constrained closer to the disk plane, the absence of a blueshift might be therefore related more to orientation than to full suppression of disk winds in RL sources by the pressure of a cocoon associated with the relativistic ejections (Norman & Miley 1984). Disk winds are probably not fully suppressed in radio-loud sources, as indicated by sources like 3C390.3 and by the discovery of fast outflows in radio-loud AGNs (Tombesi et al. 2010).

5.5. MgII λ 2800 virial broadening and virial product

The FWHM difference between H β and MgII λ 2800 is very important. From the data presented in this paper, with the exception of spectral types A3 and A4, the $\text{FWHM}(\text{H}\beta) \gtrsim \text{FWHM}(\text{MgII}\lambda 2800)$ both if the whole profile is considered or if only the broad component is isolated. The FWHM of a line by itself is of limited usefulness in computing M_{BH} following Eq. 1. A virial broadening estimator (let it be a line FWHM or velocity dispersion) should be associated to a typical distance to put in use the simple virial relation that is customarily employed in M_{BH} calculations (McLure & Dunlop 2004; Shen et al. 2008; Trakhtenbrot & Netzer 2012; Vestergaard & Peterson 2006). In principle, there are two main possibilities in the interpretation of the width differences (not mutually exclusive). The smaller MgII λ 2800 FWHM may imply that (1) MgII λ 2800 is emitted farther out from the central continuum source according to the virial law $\Delta v \propto r^{-1/2}$. If the FWHM ratio is ≈ 0.8 , then MgII λ 2800 should occur at a distance significantly larger than H β , by a factor 1.4; (2) only part of the gas emitting H β is emitting MgII λ 2800. If (1) applies the scaling relations involving MgII λ 2800 should be defined with some care since r_{BLR} defined from reverberation mapping of H β would suggest smaller distances. In the second case, MgII λ 2800 can be interpreted as perhaps the “best” estimator, associated to gas very optically thick that responds to continuum changes. Reverberation mapping studies of MgII λ 2800 are not yet conclusive, and they leave open the possibility that the average emitting distance of MgII λ 2800 is larger than for H β (Metzroth et al. 2006; Trevese et al. 2007; Woo 2008). In addition to the theoretical considerations of §5.3 that favor a larger distance for MgII λ 2800 emission, there is empirical evidence provided by the difference between the MgII λ 2800 and H β profile shape. For Pop. B sources, the H β VBC gives rise to a stronger redward asymmetry than in MgII λ 2800, and suggests that MgII λ 2800 emission is occurring farther away from the central continuum source. This is consistent with the observation of smaller $\text{FWHM}(\text{MgII}\lambda 2800)$ for both BC and whole profile for spectral type A1 and A2 that do not show appreciable VBC emission. The implication of a larger emissivity-weighted distance for MgII λ 2800 is a shift in the correlation between r_{BLR} (computed from H β) and the luminosity at 3000 Å, by ≈ 0.16 dex in r_{BLR} in Eq. 7 and Fig. 4 of Trakhtenbrot & Netzer (2012). However, Eq. 12 of Trakhtenbrot & Netzer (2012) will be unaffected since the virial factor is scaled to yield the M_{BH} derived from H β . The difference is that \mathcal{F} should be ≈ 1.0 and not $\mathcal{F} \approx 1.3 - 1.4$ that follows from the assumption that H β and MgII λ 2800 are emitted at the same distance. Scalings adopted in all previous studies assumed that a single \mathcal{F} value is appropriate for all quasars. This assumption is most likely incorrect, especially if non-gravitational forces are at play. Previous work suggested a significant \mathcal{F}

difference between Pop. A and B (Collin et al. 2006). A much needed improvement is therefore an evaluation of \mathcal{F} as a function of spectral type or L/L_{Edd} . This is however beyond the scope of the present paper.

6. Conclusion

Both $H\beta$ and $\text{MgII}\lambda 2800$ appear to be suitable for M_{BH} virial estimates of black hole mass at least for a large fraction of quasars. Both low ionization lines, however, show profile shifts and asymmetries that must be taken into account if our goal is to improve the poor present-day accuracy of most estimates. Right now, this analysis suggests that masses for Pop. B sources based on $H\beta$ are likely systematically overestimated. Further progress therefore requires subdivision of large quasar samples into Pop. A and B with further subdivision into spectral types facilitating consideration of M_{BH} and/or L/L_{Edd} trends. 4D Eigenvector 1 currently offers the most effective context for binning. Such source discrimination cannot be accomplished with L , z binning because sources with very different line profile properties show similar L_{bol} even when they host super-massive black holes with significantly different masses (i.e. the highest accretors are connected with Pop. A sources involving the smallest black hole masses—effectively blurring any expected mass-luminosity correlation for quasars).

Our ability to distinguish between Pop. A and B sources is fortunately preserved even at low s/n . We defined simple prescriptions with the goal of providing a better approximation of the virial broadening for single-epoch observations.

Acknowledgements. PM acknowledges Junta de Andalucía, through grant TIC-114 and the Excellence Project P08-TIC-3531, and the Spanish Ministry for Science and Innovation through grants AYA2010-15169 for supporting a sabbatical stay at IAA-CSIC. I. P. - F. acknowledges the postdoctoral fellowship grants 145727 and 170304 from CONACyT Mexico. Funding for the SDSS and SDSS-II has been provided by the Alfred P. Sloan Foundation, the Participating Institutions, the National Science Foundation, the U.S. Department of Energy, the National Aeronautics and Space Administration, the Japanese Monbukagakusho, the Max Planck Society, and the Higher Education Funding Council for England. The SDSS Web Site is <http://www.sdss.org/>. The SDSS is managed by the Astrophysical Research Consortium for the Participating Institutions. The Participating Institutions are the American Museum of Natural History, Astrophysical Institute Potsdam, University of Basel, University of Cambridge, Case Western Reserve University, University of Chicago, Drexel University, Fermilab, the Institute for Advanced Study, the Japan Participation Group, Johns Hopkins University, the Joint Institute for Nuclear Astrophysics, the Kavli Institute for Particle Astrophysics and Cosmology, the Korean Scientist Group, the Chinese Academy of Sciences (LAMOST), Los Alamos National Laboratory, the Max-Planck-Institute for Astronomy (MPIA), the Max-Planck-Institute for Astrophysics (MPA), New Mexico State University, Ohio State University, University of Pittsburgh, University of Portsmouth, Princeton University, the United States Naval Observatory, and the University of Washington.

References

- Assef, R. J., Denney, K. D., Kochanek, C. S., et al. 2011, *ApJ*, 742, 93
- Assef, R. J., Frank, S., Grier, C. J., et al. 2012, *ApJ*, 753, L2
- Barthel, P. D., Tytler, D. R., & Thomson, B. 1990, *A&ApS*, 82, 339
- Baskin, A. & Laor, A. 2005, *MNRAS*, 356, 1029
- Becker, R. H., White, R. L., & Helfand, D. J. 1995, *ApJ*, 450, 559
- Bentz, M. C., Denney, K. D., Grier, C. J., et al. 2013, *ApJ*, 767, 149
- Bentz, M. C., Peterson, B. M., Netzer, H., Pogge, R. W., & Vestergaard, M. 2009, *ApJ*, 697, 160
- Bentz, M. C., Walsh, J. L., Barth, A. J., et al. 2010, *ApJ*, 716, 993
- Boroson, T. A. 2002, *ApJ*, 565, 78
- Boroson, T. A. & Green, R. F. 1992, *ApJS*, 80, 109
- Brotherton, M. S. 1996, *ApJS*, 102, 1
- Brotherton, M. S., Wills, B. J., Steidel, C. C., & Sargent, W. L. W. 1994, *ApJ*, 423, 131
- Brühweiler, F. & Verner, E. 2008, *ApJ*, 675, 83
- Chen, K., Halpern, J. P., & Filippenko, A. V. 1989, *ApJ*, 339, 742
- Collin, S., Kawaguchi, T., Peterson, B. M., & Vestergaard, M. 2006, *A&Ap*, 456, 75
- Croom, S. M. 2011, *ArXiv e-prints*
- Davis, S. W. & Laor, A. 2011, *ApJ*, 728, 98
- Denney, K. D. 2012, *ApJ*, 759, 44
- Denney, K. D., Peterson, B. M., Dietrich, M., Vestergaard, M., & Bentz, M. C. 2009, *ApJ*, 692, 246
- Dietrich, M., Peterson, B. M., Grier, C. J., et al. 2012, *ApJ*, 757, 53
- Dultzin, D., Martinez, M. L., Marziani, P., Sulentic, J. W., & Negrete, A. 2011, in *Proceedings of the conference "Narrow-Line Seyfert 1 Galaxies and their place in the Universe"*. April 4-6, 2011. Milano, Italy, ed. L. F. et al. (Eds.), *Proceedings of Science*
- Elvis, M. 2000, *ApJ*, 545, 63
- Eracleous, M. & Halpern, J. P. 2003, *ApJ*, 599, 886
- Ferland, G. J., Korista, K. T., Verner, D. A., et al. 1998, *PASP*, 110, 761
- Ganguly, R. & Brotherton, M. S. 2008, *ApJ*, 672, 102
- Ganguly, R., Brotherton, M. S., Arav, N., et al. 2007, *AJ*, 133, 479
- Gaskell, C. M. 1982, *ApJ*, 263, 79
- Graham, A. W., Onken, C. A., Athanassoula, E., & Combes, F. 2011, *MNRAS*, 412, 2211
- Grandi, S. A. & Phillips, M. M. 1979, *ApJ*, 232, 659
- Greene, J. E., Peng, C. Y., Kim, M., et al. 2010, *ApJ*, 721, 26
- Grupe, D. 2004, *AJ*, 127, 1799
- Hamann, F., Shields, J. C., Ferland, G. J., & Korista, K. T. 1995, *ApJ*, 454, 688
- Hewett, P. C. & Wild, V. 2010, *MNRAS*, 405, 2302
- Ho, L. C., Goldoni, P., Dong, X.-B., Greene, J. E., & Ponti, G. 2012, *ApJ*, 754, 11
- Horne, K., Peterson, B. M., Collier, S. J., & Netzer, H. 2004, *PASP*, 116, 465
- Hu, C., Wang, J.-M., Ho, L. C., et al. 2008, *ApJ*, 687, 78
- Kaspi, S., Maoz, D., Netzer, H., et al. 2005, *ApJ*, 629, 61
- Kellermann, K. I., Sramek, R., Schmidt, M., Shaffer, D. B., & Green, R. 1989, *AJ*, 98, 1195
- Kollatschny, W. & Zetzl, M. 2013, *A&A*, 549, A100
- Kollmeier, J. A., Onken, C. A., Kochanek, C. S., et al. 2006, *ApJ*, 648, 128
- Komossa, S., Xu, D., Zhou, H., Storchi-Bergmann, T., & Binette, L. 2008, *ApJ*, 680, 926
- Korista, K. T. & Goad, M. R. 2004, *ApJ*, 606, 749
- Kovačević, J., Popović, L. Č., & Dimitrijević, M. S. 2010, *ApJS*, 189, 15
- Kriess, G. 1994, *Astronomical Data Analysis Software and Systems III*, A.S.P. Conference Series, 61, 437
- Kruczek, N. E., Richards, G. T., Gallagher, S. C., et al. 2011, *AJ*, 142, 130
- Kuraszkiewicz, J. K., Green, P. J., Forster, K., et al. 2002, *ApJS*, 143, 257
- Laor, A., Jannuzi, B. T., Green, R. F., & Boroson, T. A. 1997, *ApJ*, 489, 656
- Lewis, K. T., Eracleous, M., & Storchi-Bergmann, T. 2010, *ApJS*, 187, 416
- Marziani, P., Alenka Negrete, C., Dultzin, D., & Sulentic, J. W. 2011, *Baltic Astronomy*, 20, 406
- Marziani, P. & Sulentic, J. W. 2012, *NARev*, 56, 49
- Marziani, P., Sulentic, J. W., Dultzin-Hacyan, D., Calvani, M., & Moles, M. 1996, *ApJS*, 104, 37
- Marziani, P., Sulentic, J. W., Negrete, C. A., et al. 2010, *MNRAS*, 409, 1033
- Marziani, P., Sulentic, J. W., Plauchu-Frayn, I., & del Olmo, A. 2013, *ApJ*, 764
- Marziani, P., Sulentic, J. W., Stirpe, G. M., Zamfir, S., & Calvani, M. 2009, *A&Ap*, 495, 83
- Marziani, P., Sulentic, J. W., Zamanov, R., et al. 2003a, *ApJS*, 145, 199
- Marziani, P., Sulentic, J. W., Zwitter, T., Dultzin-Hacyan, D., & Calvani, M. 2001, *ApJ*, 558, 553
- Marziani, P., Zamanov, R. K., Sulentic, J. W., & Calvani, M. 2003b, *MNRAS*, 345, 1133
- Mathur, S. 2000, *MNRAS*, 314, L17
- Matsuoka, K., Silverman, J. D., Schramm, M., et al. 2013, *ArXiv e-prints*
- McLure, R. J. & Dunlop, J. S. 2004, *MNRAS*, 352, 1390
- McLure, R. J. & Jarvis, M. J. 2002, *MNRAS*, 337, 109

- Metzroth, K. G., Onken, C. A., & Peterson, B. M. 2006, *ApJ*, 647, 901
- Moorwood, A., Cuby, J.-G., Biereichel, P., et al. 1998, *The Messenger*, 94, 7
- Mortlock, D. J., Warren, S. J., Venemans, B. P., et al. 2011, *Nature*, 474, 616
- Negrete, A., Dultzin, D., Marziani, P., & Sulentic, J. 2012, *ApJ*, 757, 62
- Negrete, C. A. 2011, PhD thesis, UNAM, Mexico, (2011)
- Nemmen, R. S. & Brotherton, M. S. 2010, *MNRAS*, 408, 1598
- Netzer, H. 1980, *ApJ*, 236, 406
- Netzer, H. 1990, in *Active Galactic Nuclei*, ed. R. D. Blandford, H. Netzer, L. Woltjer, T. J.-L. Courvoisier, & M. Mayor, 57–160
- Netzer, H., Lira, P., Trakhtenbrot, B., Shemmer, O., & Cury, I. 2007, *ApJ*, 671, 1256
- Netzer, H. & Marziani, P. 2010, *ApJ*, 724, 318
- Norman, C. & Miley, G. 1984, *A&A*, 141, 85
- Onken, C. A., Ferrarese, L., Merritt, D., et al. 2004, *ApJ*, 615, 645
- Onken, C. A. & Kollmeier, J. A. 2008, *ApJ*, 689, L13
- Park, D., Kelly, B. C., Woo, J.-H., & Treu, T. 2012, *ApJS*, 203, 6
- Peterson, B. M., Ferrarese, L., Gilbert, K. M., et al. 2004, *ApJ*, 613, 682
- Proga, D., Stone, J. M., & Kallman, T. R. 2000, *ApJ*, 543, 686
- Punsly, B. 2013, *ApJ*, 762, L25
- Punsly, B. & Zhang, S. 2011, *ApJ*, 735, L3
- Richards, G. T., Kruczek, N. E., Gallagher, S. C., et al. 2011, *AJ*, 141, 167
- Rokaki, E., Lawrence, A., Economou, F., & Mastichiadis, A. 2003, *MNRAS*, 340, 1298
- Ross, N. P., Myers, A. D., Sheldon, E. S., et al. 2012, *ApJS*, 199, 3
- Runnoe, J. C., Brotherton, M., Shang, Z., Wills, B., & DiPompeo, M. 2012, *ArXiv e-prints*
- Sani, E., Lutz, D., Risaliti, G., et al. 2010, *MNRAS*, 403, 1246
- Schneider, D. P., Richards, G. T., Hall, P. B., et al. 2010, *AJ*, 139, 2360
- Shen, Y. 2013, *ArXiv e-prints*
- Shen, Y., Greene, J. E., Strauss, M. A., Richards, G. T., & Schneider, D. P. 2008, *ApJ*, 680, 169
- Shen, Y. & Liu, X. 2012, *ApJ*, 753, 125
- Shen, Y., Richards, G. T., Strauss, M. A., et al. 2011, *ApJS*, 194, 45
- Steinhardt, C. L., Schramm, M., Silverman, J. D., et al. 2012, *ApJ*, 759, 24
- Sulentic, J., Marziani, P., & Zamfir, S. 2011, *Baltic Astronomy*, 20, 427
- Sulentic, J. W., Bachev, R., Marziani, P., Negrete, C. A., & Dultzin, D. 2007, *ApJ*, 666, 757
- Sulentic, J. W., Marziani, P., & Dultzin-Hacyan, D. 2000a, *ARA&A*, 38, 521
- Sulentic, J. W., Marziani, P., Zamanov, R., et al. 2002, *ApJL*, 566, L71
- Sulentic, J. W., Marziani, P., Zwitter, T., Calvani, M., & Dultzin-Hacyan, D. 1998, *ApJ*, 501, 54
- Sulentic, J. W., Marziani, P., Zwitter, T., Dultzin-Hacyan, D., & Calvani, M. 2000b, *ApJL*, 545, L15
- Sulentic, J. W., Repetto, P., Stirpe, G. M., et al. 2006, *A&Ap*, 456, 929
- Sulentic, J. W., Stirpe, G. M., Marziani, P., et al. 2004, *A&Ap*, 423, 121
- Sulentic, J. W., Zamfir, S., Marziani, P., et al. 2003, *ApJL*, 597, L17
- Sulentic, J. W., Zwitter, T., Marziani, P., & Dultzin-Hacyan, D. 2000c, *ApJL*, 536, L5
- Tang, B., Shang, Z., Gu, Q., Brotherton, M. S., & Runnoe, J. C. 2012, *ApJS*, 201, 38
- Tombesi, F., Sambruna, R. M., Reeves, J. N., et al. 2010, *ApJ*, 719, 700
- Trakhtenbrot, B. & Netzer, H. 2012, *ArXiv e-prints*
- Trevese, D., Paris, D., Stirpe, G. M., Vagnetti, F., & Zitelli, V. 2007, *A&A*, 470, 491
- Tsuzuki, Y., Kawara, K., Yoshii, Y., et al. 2006, *ApJ*, 650, 57
- Tytler, D. & Fan, X.-M. 1992, *ApJS*, 79, 1
- Véron-Cetty, M.-P., Véron, P., & Gonçalves, A. C. 2001, *AAp*, 372, 730
- Vestergaard, M., Denney, K., Fan, X., et al. 2011, in *Narrow-Line Seyfert 1 Galaxies and their Place in the Universe*
- Vestergaard, M. & Peterson, B. M. 2006, *ApJ*, 641, 689
- Wang, J., Dong, X., Wang, T., et al. 2009, *ApJ*, 707, 1334
- Wang, J., Wei, J. Y., & He, X. T. 2006, *ApJ*, 638, 106
- Wild, V., Kauffmann, G., White, S., et al. 2008, *MNRAS*, 388, 227
- Wills, B. J., Brotherton, M. S., Fang, D., Steidel, C. C., & Sargent, W. L. W. 1993, *ApJ*, 415, 563
- Wills, B. J. & Browne, I. W. A. 1986, *ApJ*, 302, 56
- Woo, J.-H. 2008, *AJ*, 135, 1849
- Woo, J.-H. & Urry, C. M. 2002, *ApJ*, 579, 530
- Yip, C. W., Connolly, A. J., Vanden Berk, D. E., et al. 2004, *AJ*, 128, 2603
- Zamanov, R., Marziani, P., Sulentic, J. W., et al. 2002, *ApJL*, 576, L9
- Zamfir, S., Sulentic, J. W., & Marziani, P. 2008, *MNRAS*, 387, 856
- Zamfir, S., Sulentic, J. W., Marziani, P., & Dultzin, D. 2010, *MNRAS*, 403, 1759
- Zhang, X.-G. 2011, *MNRAS*, 416, 2857
- Zhou, H., Wang, T., Yuan, W., et al. 2006, *ApJS*, 166, 128

Table 1. Sample: number of sources in each spectral type

Sp. Type	N_{tot}	N_{RQ}^{a}	$N_{\text{FIRST}}^{\text{b}}$	$N_{\text{FRII}}^{\text{c}}$	N_{CD}^{d}
A1	97	79	24	10	8
A2	156	152	20	1	3
A3	43	39	14	0	4
A4	15	13	4	0	2
B1	218	179	58	23	16
B1 ⁺	115	95	27	11	9
B1 ⁺⁺	17	9	11	4	4
B2	19	16	5	0	3
All	680	582	163	49	49

^a Number of radio-quiet sources defined as $N_{\text{RQ}} = N_{\text{tot}} - N_{\text{CD}} - N_{\text{FRII}}$.

^b **Number of FIRST-detected sources. Note that $N_{\text{FIRST}} > N_{\text{CD}} + N_{\text{FRII}}$.**

^c Number of FIRST-detected sources with compact morphology and emitted rest frame power $\log P_{\nu} \geq 31.6$ (P_{ν} in units of $\text{erg s}^{-1} \text{Hz}^{-1}$).

^d Number of FIRST-detected sources with extended morphology.

Table 2. Measured Parameters on the H β and MgII λ 2800 Profiles of Composite Spectra

Sp. Type	H β								MgII λ 2800							
	FWHM ^a	A.I. ^b	κ^c	$c(\frac{1}{4})^{a,d}$	$c(\frac{1}{2})^{a,d}$	$c(\frac{3}{4})^{a,d}$	$c(0.9)^{a,d}$		FWHM ^a	A.I. ^b	κ^c	$c(\frac{1}{4})^{a,d}$	$c(\frac{1}{2})^{a,d}$	$c(\frac{3}{4})^{a,d}$	$c(0.9)^{a,d}$	
<i>Pop. A Full Sample</i>																
A1	3180 \pm 90	0.00 \pm 0.04	0.33 \pm 0.02	50 \pm 110	50 \pm 60	50 \pm 40	110 \pm 50		3040 \pm 80	0.01 \pm 0.04	0.36 \pm 0.02	80 \pm 100	80 \pm 50	70 \pm 40	60 \pm 50	
A2	2900 \pm 210	0.00 \pm 0.10	0.33 \pm 0.04	-20 \pm 240	-20 \pm 110	-20 \pm 90	-40 \pm 110		2600 \pm 160	0.01 \pm 0.09	0.38 \pm 0.04	-60 \pm 200	-70 \pm 90	-70 \pm 80	-80 \pm 100	
A3	2510 \pm 200	-0.15 \pm 0.10	0.30 \pm 0.04	-330 \pm 230	-90 \pm 110	-10 \pm 80	30 \pm 90		2560 \pm 160	0.01 \pm 0.09	0.38 \pm 0.04	-140 \pm 200	-140 \pm 90	-150 \pm 80	-160 \pm 100	
A4	2530 \pm 250	-0.23 \pm 0.10	0.27 \pm 0.04	-530 \pm 250	-150 \pm 130	10 \pm 80	80 \pm 100		2970 \pm 210	0.01 \pm 0.09	0.35 \pm 0.04	-240 \pm 220	-250 \pm 120	-250 \pm 90	-260 \pm 130	
<i>Pop. B Full Sample</i>																
B1	7050 \pm 180	0.09 \pm 0.04	0.38 \pm 0.02	660 \pm 230	220 \pm 100	140 \pm 80	240 \pm 110		5300 \pm 120	0.07 \pm 0.03	0.42 \pm 0.02	230 \pm 140	10 \pm 70	-40 \pm 70	-60 \pm 90	
B1 ⁺	9420 \pm 220	0.08 \pm 0.03	0.40 \pm 0.02	790 \pm 220	380 \pm 120	250 \pm 110	430 \pm 150		7480 \pm 170	0.06 \pm 0.03	0.41 \pm 0.02	380 \pm 180	140 \pm 100	70 \pm 90	50 \pm 120	
B1 ⁺⁺	13080 \pm 720	0.04 \pm 0.06	0.43 \pm 0.04	600 \pm 570	400 \pm 360	290 \pm 350	480 \pm 480		9360 \pm 490	0.02 \pm 0.06	0.45 \pm 0.04	100 \pm 360	30 \pm 240	0 \pm 250	-10 \pm 350	
B2	5470 \pm 340	0.15 \pm 0.14	0.35 \pm 0.06	680 \pm 650	60 \pm 180	-30 \pm 160	-100 \pm 200		3950 \pm 230	0.10 \pm 0.11	0.39 \pm 0.05	120 \pm 360	-130 \pm 130	-180 \pm 120	-200 \pm 150	
<i>Radio Loud</i>																
B1 CD	7060 \pm 460	0.16 \pm 0.04	0.36 \pm 0.02	1230 \pm 230	440 \pm 230	310 \pm 80	500 \pm 240		5690 \pm 330	0.10 \pm 0.03	0.39 \pm 0.02	590 \pm 160	270 \pm 170	180 \pm 70	160 \pm 210	
B1 FRII	6790 \pm 410	0.09 \pm 0.05	0.37 \pm 0.02	850 \pm 260	420 \pm 200	330 \pm 80	620 \pm 250		5500 \pm 300	0.05 \pm 0.03	0.43 \pm 0.02	230 \pm 120	100 \pm 160	50 \pm 80	30 \pm 210	

^a In units of km s⁻¹.^b Dimensionless asymmetry index computed at $\frac{1}{4}$ peak intensity.^a Dimensionless kurtosis index defined as the ratio between the full width at $\frac{3}{4}$ and $\frac{1}{4}$ maximum.^d Centroids at $\frac{1}{4}$, $\frac{1}{2}$, $\frac{3}{4}$ and $\frac{9}{10}$ maximum intensity.

Table 3. Derived Quantities from the H β and MgII λ 2800 Profiles Composite Spectra Multicomponent Analysis

Sp. Type	H β						MgII λ 2800					
	BC ^a	Shift ^b	FWHM ^b	VBC ^a	Shift ^b	FWHM ^b	BC ^a	Shift ^b	FWHM ^b	VBC ^a	Shift ^b	FWHM ^b
<i>Pop. B Full Sample</i>												
B1	46	20 ^c	5720 \pm 100	51	1740 \pm 150	15600 \pm 150	63	-165 \pm 50	4620 \pm 100	36	2160 ^c	11500 \pm 300
B1 ⁺	46	5 ^c	7750 \pm 200	45	1920 \pm 190	15700 \pm 260	68	-60 \pm 80	6330 \pm 100	51	1520 ^c	14500 \pm 1230
B1 ⁺⁺	28	-165 ^c	10100 \pm 420	65	915 \pm 70	15830 \pm 860	82	-105 ^c	8870 \pm 420	20	1305 ^c	13000 ^c
B2	33	-120 \pm 60	4410 \pm 100	40	1950 \pm 280	13400 \pm 600	43	-240 \pm 40	3220 \pm 240	38	1420 \pm 540	10000 ^c
PG 1201+436	42 ^d	-5 ^c	7500 ^c	179 ^d	2125 \pm 370	11800 \pm 770	118 ^d	0 ^c	7220 \pm 590	94 ^d	1790 \pm 330	9780 \pm 740
<i>Radio Loud</i>												
B1 CD	34	80 ^c	5330 \pm 200	50	1935 \pm 190	13160 \pm 260	60	45 \pm 60	4680 \pm 120	51	1630 ^c	11000 ^c
B1 FRII	47	235 \pm 55	5370 \pm 130	60	1645 \pm 170	15450 \pm 530	74	-55 \pm 70	4790 \pm 200	37	1630 ^c	11000 ^c

^a Line intensity normalized to the continuum at 5080 Å. The value roughly corresponds to the rest-frame equivalent width in Å for H β . **Intensity ratios within each spectral type can be computed from the reported values.**

^b In units of km s⁻¹.

^c Kept fixed or allowed to vary within a narrow interval in SPECFIT analysis.

^d In units of 10⁻¹⁵ erg s⁻¹ cm⁻² Å⁻¹

Table 4. Median bolometric luminosity, black hole mass and Eddington ratio

Sp. Type	$L_{\text{bol}}^{\text{a}}$	BC only				Whole profile			
		M_{BH}^{b}	M_{BH}^{b}	$L/L_{\text{Edd}}^{\text{c}}$	$L/L_{\text{Edd}}^{\text{c}}$	M_{BH}^{b}	M_{BH}^{b}	$L/L_{\text{Edd}}^{\text{c}}$	$L/L_{\text{Edd}}^{\text{c}}$
		H β	MgII λ 2800	H β	MgII λ 2800	H β	MgII λ 2800	H β	MgII λ 2800
<i>Pop. A Full Sample</i>									
A1	46.18	8.67	8.62	-0.60	-0.56	8.67	8.71	-0.60	-0.64
A2	46.16	8.57	8.45	-0.53	-0.40	8.57	8.57	-0.52	-0.52
A3	46.15	8.33	8.41	-0.28	-0.37	8.45	8.53	-0.41	-0.49
A4	46.20	8.27	8.56	-0.18	-0.47	8.48	8.66	-0.39	-0.57
<i>Pop. B Full Sample</i>									
B1	46.13	9.15	8.98	-1.13	-0.96	9.33	9.08	-1.31	-1.06
B1 ⁺	45.96	9.29	9.06	-1.44	-1.21	9.46	9.18	-1.61	-1.33
B1 ⁺⁺	45.96	9.53	9.14	-1.68	-1.29	9.75	9.35	-1.90	-1.50
B2	46.23	8.99	8.74	-0.87	-0.62	9.17	8.89	-1.05	-0.77

^a Decimal logarithm of bolometric luminosity in units of ergs s⁻¹. A bolometric correction computed following Nemmen & Brotherton (2010) was applied to the 5100 Å specific luminosity.

^b Decimal logarithm of black hole mass in solar units. M_{BH} has been estimated from the relation of Shen & Liu (2012) for MgII λ 2800 and from the relation Assef et al. (2011) for H β .

^c Decimal logarithm of Eddington ratio.

Table 5. Conversion factors

	$\xi(\text{H}\beta)^{\text{a}}$	$\xi(\text{MgII}\lambda 2800)^{\text{a}}$	$\text{MgII}\lambda 2800_{\text{BC}} / \text{H}\beta_{\text{obs}}$	$\text{MgII}\lambda 2800_{\text{obs}} / \text{H}\beta_{\text{BC}}$
A2	1.00	1.00	0.76	0.90
A1	1.00	1.00	0.85	0.96
B1	0.81	0.87	0.66	0.93
B1 CD	0.75	0.82	0.66	1.07
B1 FRII	0.79	0.87	0.71	1.02
B1 ⁺	0.82	0.85	0.67	0.97
B1 ⁺⁺	0.77	0.95	0.68	0.93

^a Conversion factor ξ is the FWHM of BC divided by the FWHM of the full (“observed”) profile. The MgII λ 2800 doublet is treated as a single feature.

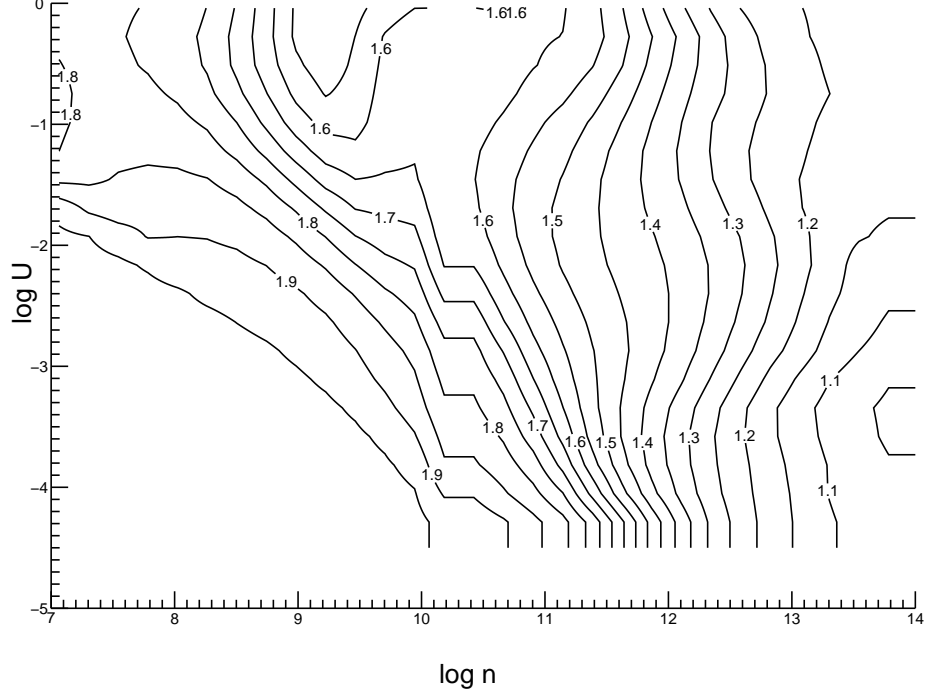


Fig. 1. Predicted intensity ratio of the doublet the Mg⁺ lines as a function of ionization parameter U and hydrogen density n_H . Contour lines are drawn at steps of 0.1 from 1.0 to 2.0.

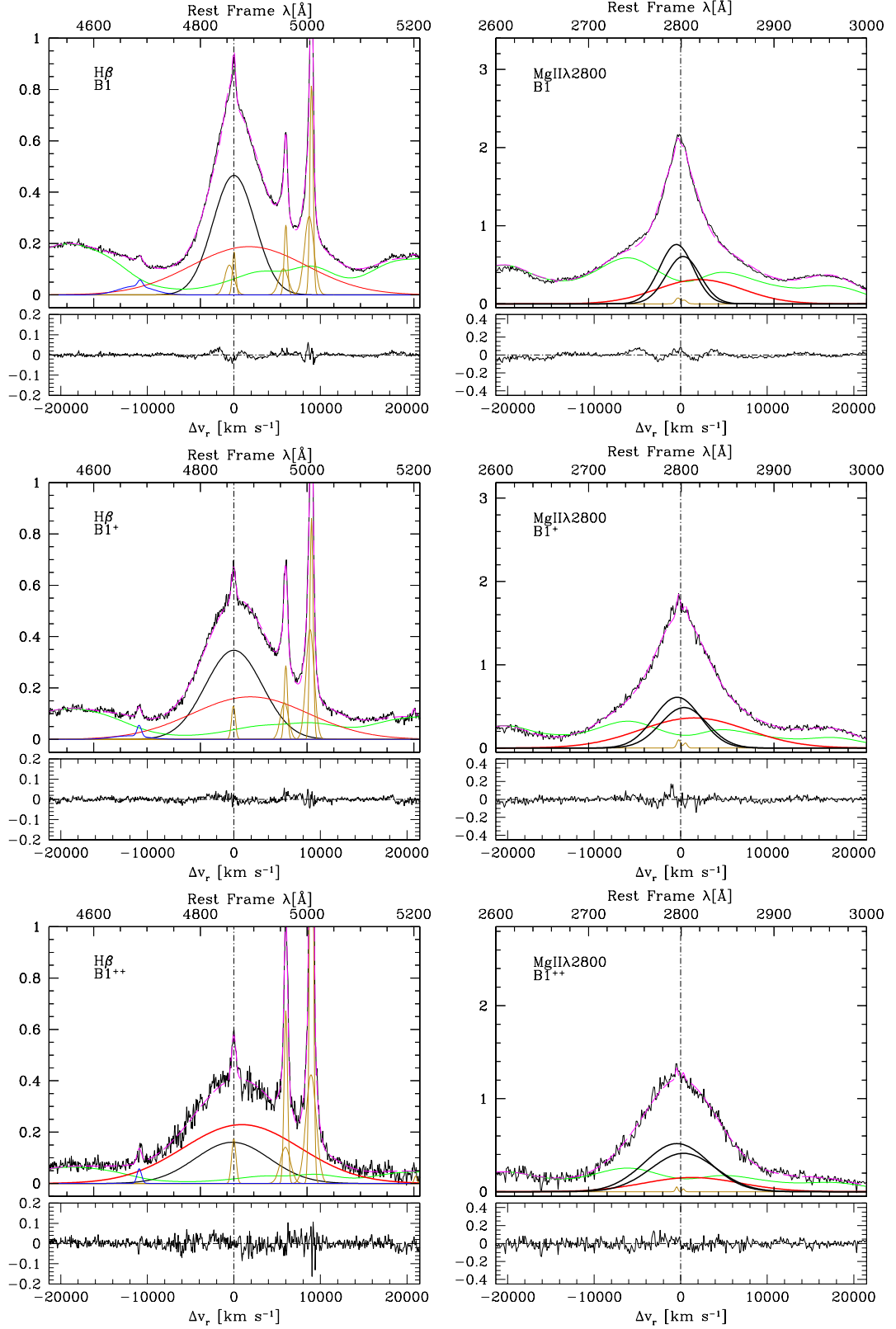


Fig. 2. Spectra of $H\beta$ (left panels) and of $MgII\lambda 2800$ (right panels) for spectral types B1 to B1⁺⁺ (from top to bottom). The horizontal scales are in rest frame wavelength [\AA] or radial velocity, with the origin set at the rest frame wavelength. The black lines show the original, continuum-subtracted spectrum, while the dashed magenta line shows the model with all emission line components. The thick black line is the BC; the thick red line shows the VBC. The green lines trace the $Fe II_{opt}$ and $Fe II_{UV}$ contribution, and the gold lines various contributions associated to the NLR ($H\beta_{NC}$, $[OIII]\lambda\lambda 4959, 5007$, and $MgII\lambda 2800$ narrow component when appropriate). Excess emission at $\lambda \gtrsim 2900\text{\AA}$ visible in this and in the next two Figures is likely due to a combination of FeI and Balmer continuum emission.

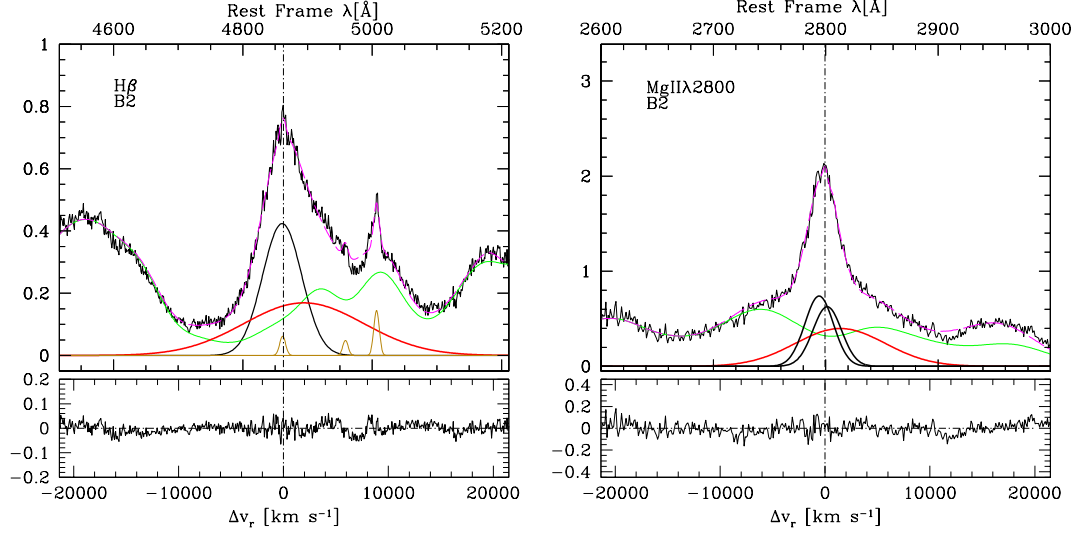


Fig. 3. Spectra of H β (left) and of MgII λ 2800 (right) for spectral type B2. Meaning of symbols/line colors is the same of the previous Figure.

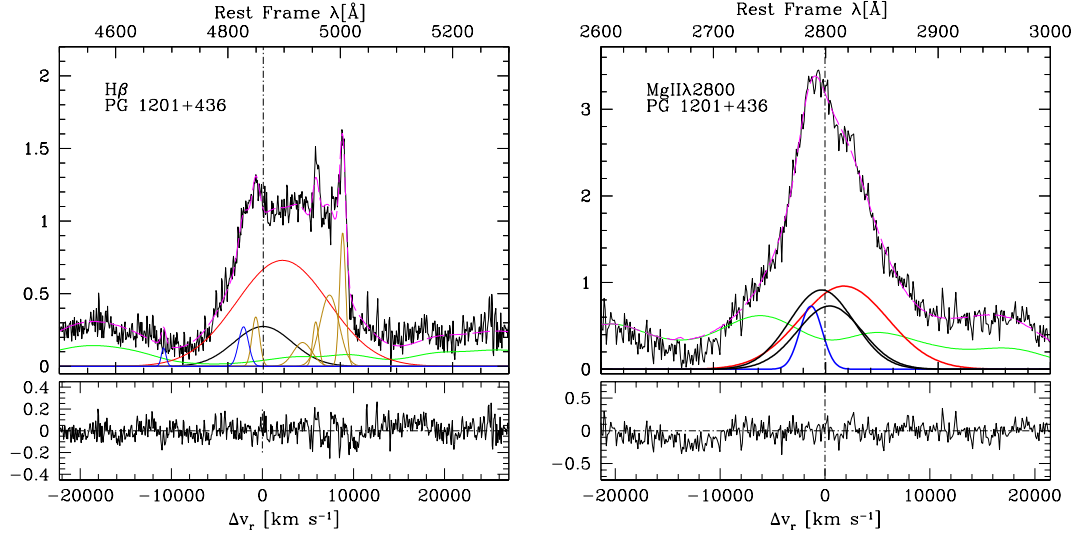


Fig. 4. Spectrum of H β (left panels) and of MgII λ 2800 (right panels) for the B1⁺⁺ source PG 1201+436. Color coding is the same as for Fig. 2 save for the blue line that traces a blueshifted peak visible in both H β and MgII λ 2800 (§4 and 5.3). Horizontal scale is rest frame wavelength or radial velocity shift from rest frame. Vertical scale is specific flux in units of 10^{-15} erg s⁻¹ cm⁻² Å⁻¹.

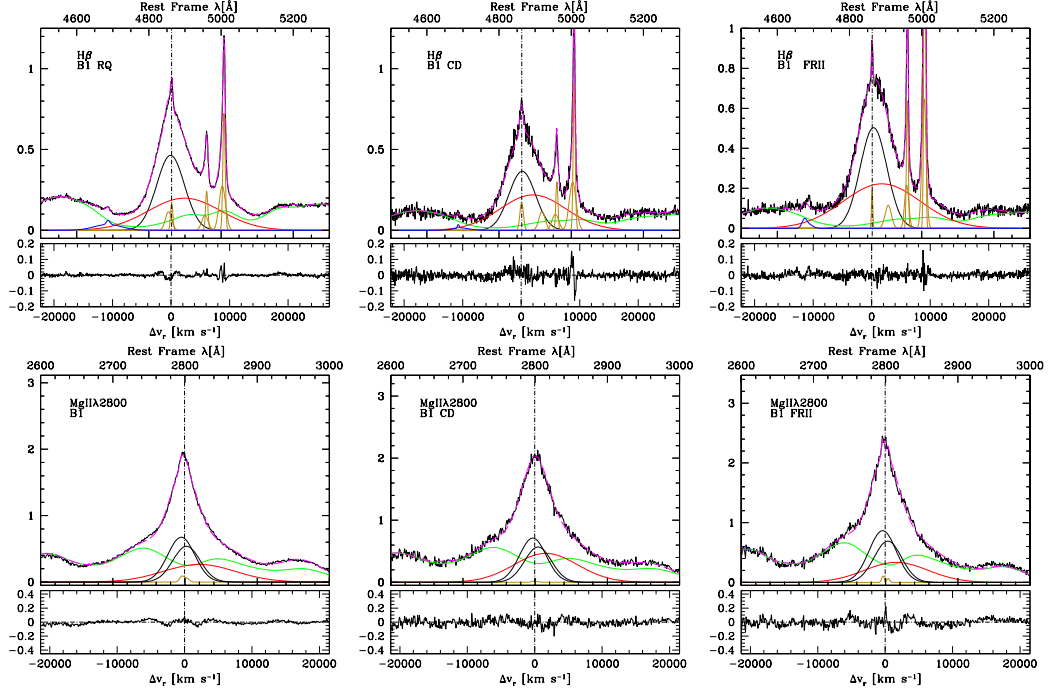


Fig. 5. Continuum subtracted spectral ranges of $H\beta$ (top) and $MgII\lambda 2800$ (bottom) for RQ (left), CD (middle) and FRII (right) median composites computed in the B1 bin. Meaning of symbols is the same of the previous Figures.

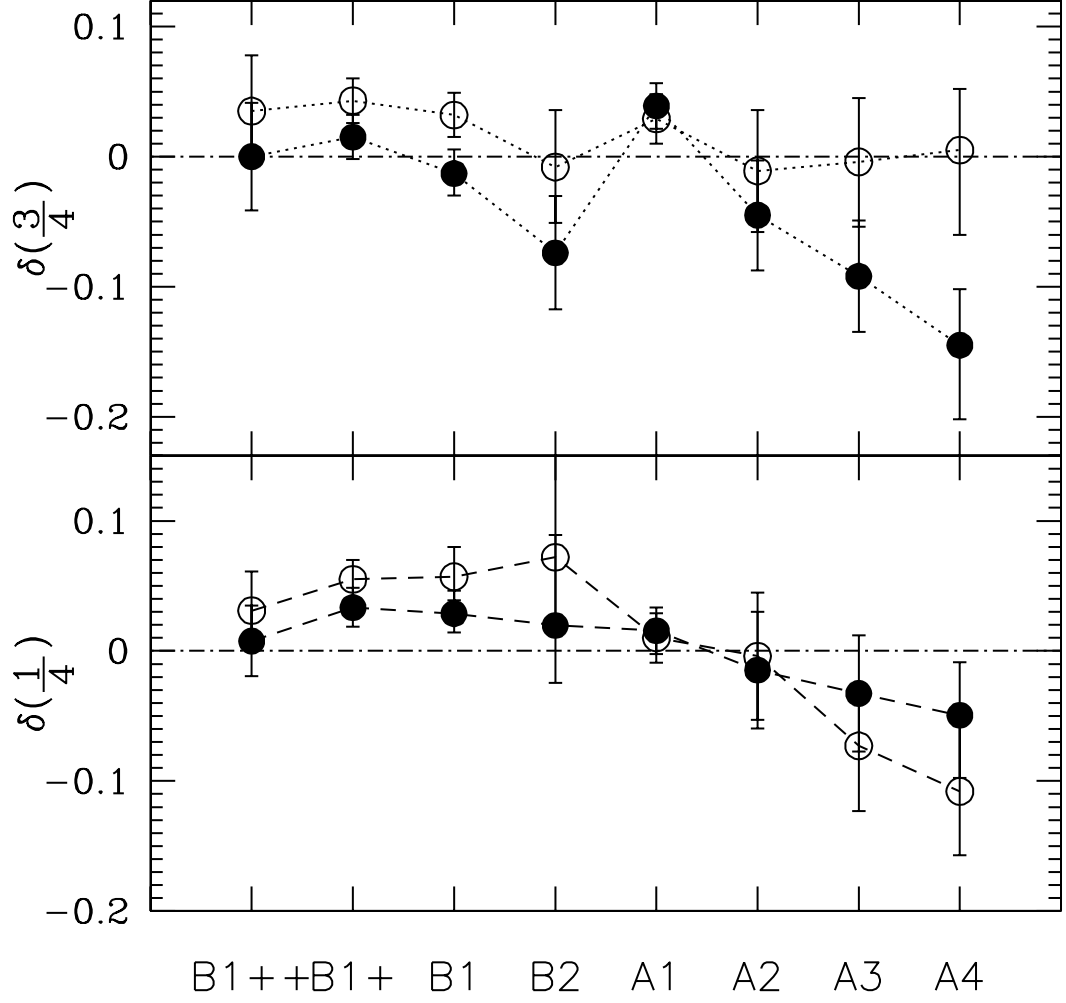


Fig. 6. Trends in Pop. A and B as a function of spectral type. The upper panel shows the normalized shift $\delta(\frac{3}{4})$, the lower $\delta(\frac{1}{4})$. Filled symbols: MgII λ 2800; open symbols: H β .

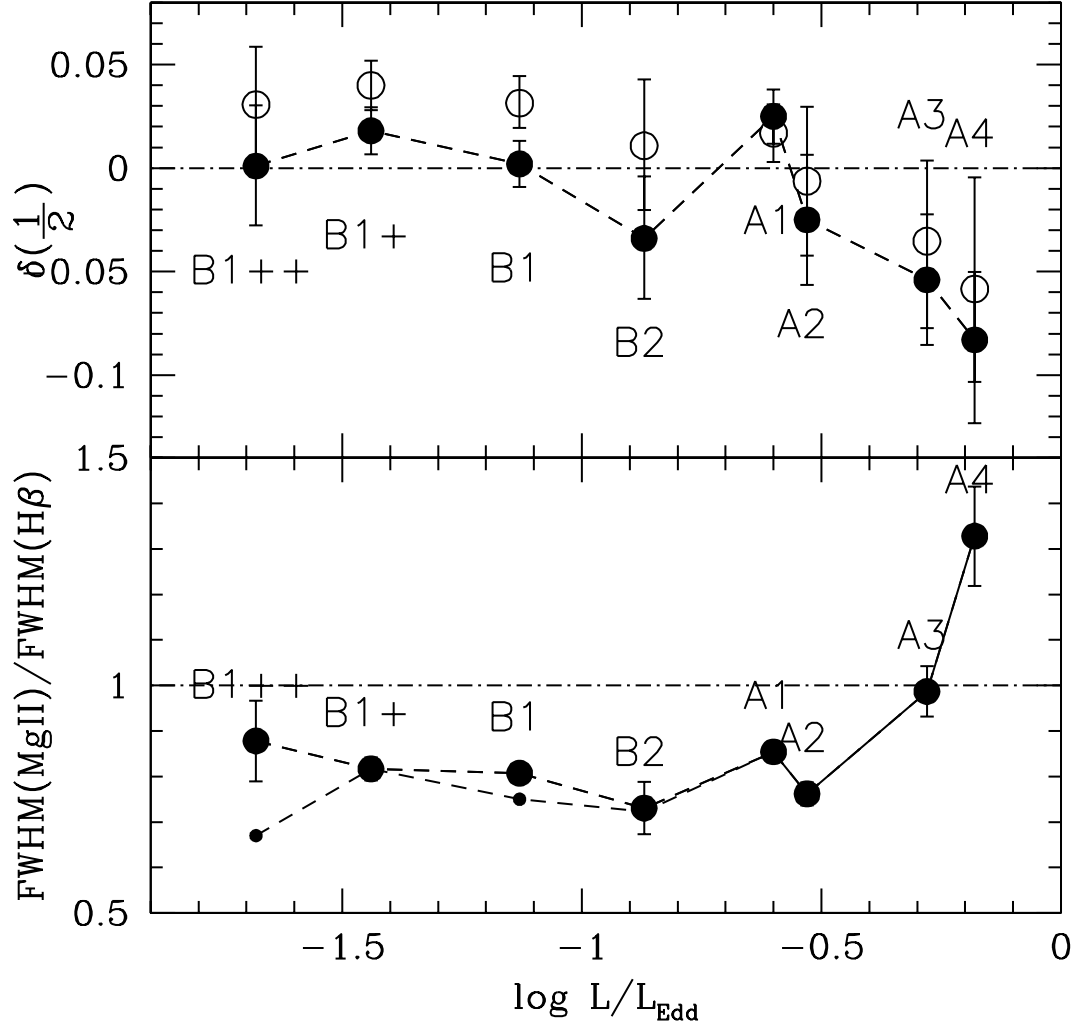


Fig. 7. Trends as a function of Eddington ratio L/L_{Edd} . Upper panel: “dynamical relevance” indicator $\delta(\frac{1}{2}) = c(\frac{1}{2})/\text{FWHM}$ for the $\text{MgII}\lambda 2800$ doublet broad component. Bottom panel: ratio $\text{FWHM}(\text{MgII}\lambda 2800)/\text{FWHM}(\text{H}\beta)$ for the broad components. The smaller circles refer to measurements made including the VBC contribution of both lines.

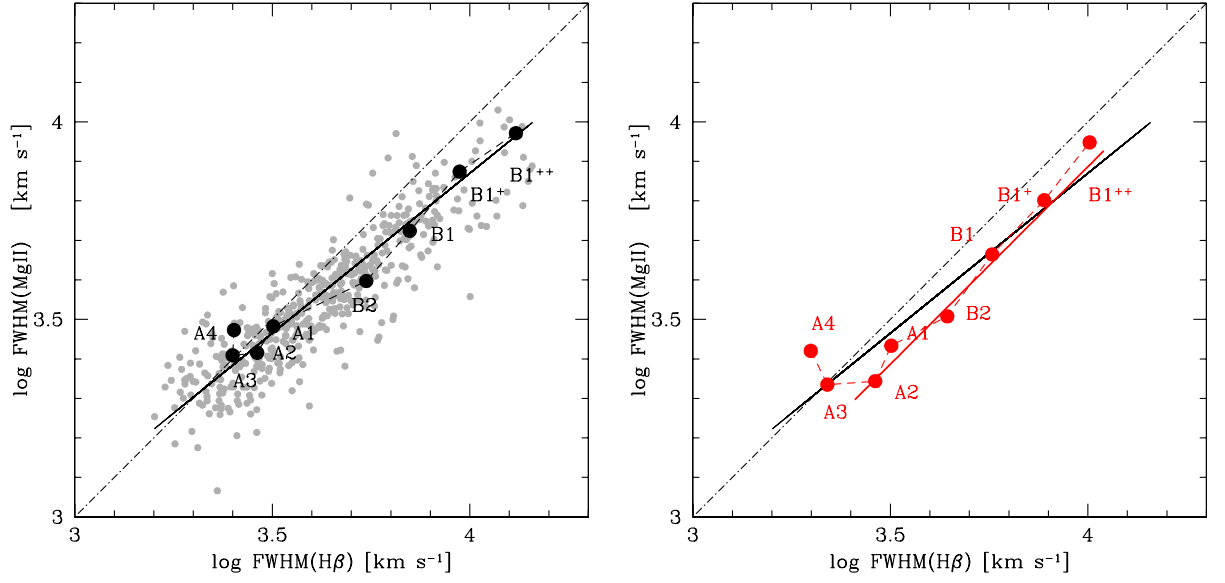


Fig. 8. FWHM of MgII λ 2800 vs FWHM H β in log scale. Left: full profiles, right: only BC (of single component for MgII λ 2800). Grey dots are the data points of Wang et al. (2009), with the line representing their best fit. The large black spots are the median values for the full profiles of our median spectra. The dot-dashed lines traces the equality relation, and the thin red line a fixed ratio 0.77.

List of Objects

‘PG 1201+436’ on page 9
‘PG 1416–129’ on page 10
‘PG 1201+436’ on page 10
‘3C 390.3’ on page 16
‘SDSS 0956+5128’ on page 16
‘PG 1201+436’ on page 16
‘PG 1201+436’ on page 16